American Mineralogist, Volume 92, pages 1–18, 2007

Mid-infrared emission spectroscopy of sulfate and sulfate-bearing minerals

MELISSA D. LANE*

Planetary Science Institute, 1700 E. Fort Lowell Road, Suite 106, Tucson, Arizona 85719, U.S.A.

ABSTRACT

Mid-infrared thermal emission spectra were acquired and are presented for 37 different sulfate minerals representing Strunz classes 6/A-D as well as a few other miscellaneous sulfate-bearing minerals (Strunz class 3/C and 8/J). Sulfate vibrational modes are assigned to each spectrum; also assigned are the modes of component OH, H_2O, and carbonate where applicable. A discussion also is presented regarding the effect of hydration state on the emissivity spectra; dehydration of the Ca-sulfate mineral series (e.g., gypsum-bassanite-anhydrite), as well as the Mg-sulfate series, causes the high-frequency edge of the sulfate ν_3 band to shift to a larger wavenumber.

Keywords: Mid-infrared, vibrational, spectroscopy, emissivity, emission, sulfate, spectra

INTRODUCTION

Approximately 370 sulfate-mineral species are known to exist in nature (Hawthorne et al. 2000). Sulfate minerals are found in a variety of geologic settings, including volcanic, hydrothermal, evaporitic, and chemical-weathering environments. Some sulfate species are specific to single formational chemical environments, but others can form in several. Sulfates are formed in the presence of water of varying acidities and temperatures. In high-temperature volcanic and hydrothermal settings, metal-sulfate salts are common around active crater lakes, fumaroles, and hot springs, and may form volcanic aerosol particles. In low-temperature evaporite settings, preserved textural relationships (precipitation fabrics) between the sulfates and other salts can provide information regarding the precipitation sequence and mineral chemistry, thereby providing insight into the chemistry of the (sometimes ancient) surface waters. Chemical weathering can produce sulfate minerals that are entrained in soil or as crusts (or efflorescence) on host materials.

Sulfate minerals may be distinguished using thermal infrared (mid-infrared) spectroscopy. Early mid-infrared spectroscopic studies have shown that the aqueous sulfate anion (SO_4^{2-}) produces four infrared absorption features at ~1105, ~983, ~611, and ~450 cm^{-1} (corresponding to the asymmetric stretch, ν_3; symmetric stretch, ν_1; asymmetric bend, ν_4; symmetric bend, ν_2, respectively) (Nakamoto 1986; also see Herzberg 1945; Hug 1997) of which only ν_3 and ν_4 are infrared active. These vibrations are modified when the sulfate anion is present within a solid-state medium, such as a mineral with a repeating molecular order, resulting in the potential appearance of all four sulfate vibrational modes in the spectrum.

The objective of this study is to present and discuss the mid-infrared emissivity spectra of a variety of sulfate-bearing minerals. A large suite of spectra are included to discuss the emissivity variations that arise over the mid-infrared wavelengths due to differences in chemistry, including hydration state of the samples. The results of this study will aid the interpretation of thermal-infrared spectral data acquired in laboratories and those data acquired remotely of the Earth and other planetary bodies. The results of this study will be particularly relevant to the remote study of Mars, on which sulfate bedrock and sulfate-rich soils have been identified (e.g., Squyres et al. 2004; Squyres and Knoll 2005), and for which mid-infrared spectral data are plentiful (e.g., Christensen et al. 2001, 2003, 2004). Remote identification of specific sulfate minerals on Earth or elsewhere would enable the geologic setting in which the mineral formed to be determined. The spectra presented in this work are available through the Arizona State University Thermal Emission Spectral Library (http://speclib.asu.edu).

SAMPLE DESCRIPTIONS

For this study, 62 sulfate-bearing mineral samples were studied, representing 37 different minerals (Table 1) that are reasonably common, available, and stable. These include the samples: afghanite, alunite, anglesite, anhydrite, antlerite, aphthitalite (glaserite), apjohnite, barite, bassanite (hemihydrate), bloedite (blodite), brochantite, burkeite, celestine (celestite), coquimbite/paracoquimbite, creedite, ferricopiapite, glauberite, gypsum, hanksite, hexahydrite, jarosite, kainite, kieserite, linarite, minamiite, natrojarosite, pickeringite, plumbojarosite, polyhalite, potassium alum (potash alum; kalinite), rozenite, serpierite, sulfohalite, szomolnokite, thaumasite, thenardite, and zincobotryogen.

To confirm the mineralogic identification, all of the samples were analyzed by powder X-ray diffraction (XRD). The samples range in physical state from hand samples that are well-crystalline and dense, to less dense hand samples that are consolidated crystallites, to coatings, to loose particulate samples (powders) (Table 1).

EXPERIMENTAL METHODS

The samples in this study were analyzed in thermal emission at ambient pressure using the Mars Space Flight Facility at Arizona State University. The spectrometer used is a modified Nicolet Nexus 670 E.S.P. FT-IR interferometer attached to an external glove box containing a temperature-stabilized sample chamber (maintained with circulating water behind the chamber wall). This spectrometer is equipped with a thermoelectrically stabilized DTGS detector and a CsI beam splitter

* E-mail: lane@psi.edu

0003-004X/07/0001–1$05.00/DOI: 10.2138/am.2007.2170

TABLE 1. Listing of the sulfate-bearing minerals

Mineral *	Stoichiometric Composition	Sample and character ***†	Locale
Afghanite‡	$(Na, Ca, K)_8(Si, Al)_{12}O_{24}(SO_4, Cl, CO_3)\cdot 12H_2O$	**S26, xl, cg**	Sar-e-Sang, Badakhshan, Afghanistan
Alunite	$K_2Al_6(SO_4)_4(OH)_{12}$	S14	Sugar Loaf Butte, near Quartzite, AZ
		S32	Marysvale, Piute Co., UT
		S44, m, cg	Marysvale, Piute Co., UT
Anglesite§	$PbSO_4$	**S53, xl, cg**	Excepcion Mine, Villa Ahumada, Chihuahua, Mexico
Anhydrite	$CaSO_4$	S9	Near Carson City, NV
		S16, m, cg	Near Carson City, NV
Antlerite	$Cu_3(SO_4)(OH)_4$	**S10, m, cg**	Morenci, Greenlee Co., AZ
		S72	Chuqicamata, Chile
Aphthitalite (Glaserite)	$(K,Na)_3Na(SO_4)_2$	**S30, xl, cg**	Kuh-e-Namak, Region de Qom, Iran
Apjohnite‖	$MnAl_2(SO_4)_4\cdot 22H_2O$	**S38, cg, f**	Kern Co., CA
Barite	$BaSO_4$	S1	Potosi, MO
		S2, m, cg	Northumberland Mine, Toquima Mtns., Nye Co., NV
Bassanite (Hemihydrate)	$CaSO_4\cdot 1/2\ H_2O$	S7	Near St. George, Wahsington Co., UT
		S11, m, fg	Locale unknown
Bloedite (Blodite)	$Na_2Mg(SO_4)_2\cdot 4H_2O$	**S33, xl, cg**	Soda Lake, San Luis Obispo Co., CA
Brochantite	$Cu_4(SO_4)(OH)_6$	**S29, c, xl**	Ora Blanchard Claims, Blanchard Mine, Bingham, NM
		S34	Douglas Hill Copper Mine, Lyon Co., NV
Burkeite	$Na_6CO_3(SO_4)_2$	**S71, m, fg, pc**	Searles Lake, San Bernardino Co., CA
Celestine (Celestite)	$SrSO_4$	**S3, f, cg**	Near Calico, San Bernardino Co., CA
		S13	Maybee, MI
Coquimbite#	$Fe_2(SO_4)_3\cdot 9\ H2O$	**S46, m, cg**	Alcaparrosa, Chile
		S63	Atacama, Chile
Creedite	$Ca_3Al_2SO_4(F,OH)\cdot 2H_2O$	S28	Navidad, Durango, Mexico
		S36, xl, cg	Aguiles Serdan, Chihuahua, Mexico
Ferricopiapite	$(Fe,Al,Mg)Fe_5(SO_4)_6(OH)_2\cdot 20H_2O$	**S35, m, fg, pc**	Sierra Gorda, Chile
Glauberite	$Na_2Ca(SO_4)_2$	**S37, xl, cg**	Lake Bumbunga, near Lochiel, S.A., Australia
		S52	Bertram Siding, Salton Sea, Imperial Co., CA
Gypsum**	$CaSO_4\cdot 2\ H_2O$	S5	Near St. George, Washington Co., UT
		S6	Mule Canyon, near Calico, San Bernardino Co., CA
		S8, xl, cg	Near White City, Eddy Co., NM
		S18	Near White City, Eddy Co., NM
		S24	Locale unknown
Hanksite	$KNa_{22}(SO_4)_9(CO_3)_2Cl$	**SL2, xl, cg**	Searles Lake, Trona, CA
		SL3	Searles Lake, Trona, CA
		SL7	Searles Lake, Trona, CA
"Hexahydrite" (likely kieserite)	$MgSO_4\cdot 6\ H_2O$	**152959, m, fg, pc**	Lehrite, Niedersachsen, Germany
Jarosite	$KFe_3(SO_4)_2(OH)_6$	S39	Barranco del Jarosa, Sierra Akmagrera, Spain
		S51, m, fg, c	Copiapo Jarosite Mine, Dona Ana Co., NM
Kainite	$KMgSO_4Cl\cdot 3H_2O$	**S40, m, cg**	Stassfurt, Harz, Germany
Kieserite	$MgSO_4\cdot H_2O$	**C5492-1, m, fg, pc**	Oficiana, Vegara, Chile
Linarite††	$PbCu(SO_4)(OH)_2$	**S27, xl, c**	Sunshine Mine, Bingham, NM
Minamiite‡‡	$(Na,Ca,K)_2Al_6(SO_4)_4(OH)_{12}$	**S76, m, fg**	Big Star Deposit, Maryvale, Piute Co., Utah
Natrojarosite	$NaFe_3(SO_4)_2(OH)_6$	**S48, m, fg, pc**	Sulfur Hole, Borate, San Bernardino Co., CA
Pickeringite§§	$MgAl_2(SO_4)_4\cdot 22\ H_2O$	**S49, f, cg**	Corral Hollow, Alameda Co., CA
Plumbojarosite‖‖	$PbFe_6(SO_4)_4(OH)_{12}$	**S15, fg, p**	Lomo de Toro Mine, Zimapan Hidalgo, Mexico
Polyhalite	$K_2Ca_2Mg(SO_4)_4\cdot 2H_2O$	**S50, m, fg**	NE of Carlsbad, Eddy Co., NM
Potassium Alum (Kalinite)	$KAl(SO_4)_2\cdot 12H_2O$	**S75, m, fg, pc**	Westeregeln, Niedersachsen, Germany
Rozenite	$FeSO_4\cdot 4H_2O$	**JB626, m, cg, pc**	Iron Mountain, CA
Serpierite##	$Ca(Cu,Zn)_4(SO_4)_2(OH)_6\cdot 3H_2O$	**S61, xl, c**	Bayhorse Mine, Challis, Custer Co., ID
Sulfohalite	$Na_6(SO_4)_2FCl$	SL8	Searles Lake, Trona, CA
		S54, xl, cg	Searles Lake, near Trona, San Bernardino Co., CA
Szomolnokite	$FeSO_4\cdot H_2O$	S60	Markey Mine, Red Canyon, San Juan Co., UT
		S78	Getchell Mine, near Golconda, Humboldt Co., NV
		104276, xl, cg	Tintic Standard Mine, Dividend, UT
Thaumasite	$Ca_3Si(CO_3)(SO_4)(OH)_6\cdot 12H_2O$	**S47, m, cg**	Fairfax Quarry, near Centerville, Fairfax Co., VA
		S74	Paterson, Passaic Co., NJ
Thenardite	Na_2SO_4	**S22, m, cg**	Salt Mine, Camp Verde, AZ
		S25	Soda Lake, San Benito Co., CA
		S66	Camp Verde salt deposit, Yavapai Co., AZ
		SL16	Searles Lake, CA
Zincobotryogen	$ZnFe(SO_4)_2(OH)\cdot 7H_2O$	**C5525-3, m, cg**	Mina Quetana, Calama, Chile

* XRD data (to determine composition) were acquired mostly using a Rigaku Geigerflex powder diffractometer (at 40 kV and 35 mA) at a commercial lab (K/T GeoServices) using Cu*K*α radiation and a 0.02° step size over the 2θ collection. Several samples were measured at Mount Holyoke College using a Rigaku Miniflex diffractometer and one (S46) was measured at Indiana University.

† Bold sample number denotes the sample whose spectrum is shown in the spectral-group figures.

‡ Composition assured by vendor (and a mineral example from the same vendor [Dan Weinrich Fine Minerals] and sample location is pictured on http://www.webmineral.com/data/Afghanite.shtml).

§ Sample S53 contains minor Celestine.

‖ Sample S38 contains minor Kalinite/Halotrichite/Pickeringite.

Sample S46 contains subequal amounts of coquimbite and paracoquimbite.

** Sample S8 used to study particle-size effects; contains minor amount of bassanite.

†† Sample not pure: contains Pb-carbonate contaminant (cerussite).

‡‡ Sample not pure: approximately 90% minamiite, 8% alunite, 2% other.

§§ Sample S49 contains Kalinite/Apjohnite/Halotrichite.

‖‖ Sample not pure: may contain goethite and other minerals.

Composition confirmed by in-house analysis from sample provider [Excalibur Mineral Company].

*** Character of sample where m = massive, fg = fine-grained, cg = coarse-grained, xl = crystal form/faces visible (crystals at various orientations), pc = poorly consolidated; friable, c = coating, f = fibrous; p = particulate.

that allows the measurement of emitted radiation over the mid-infrared range of 2000 to 220 cm^{-1} (5 to 45 μm). To reduce and maintain the amount of atmospheric water and CO_2 vapor inside the spectrometer, external sample chamber, and glove box (and to reduce the degradation of the hydrophilic CsI beam splitter), the entire system is continuously purged with air scrubbed of water and CO_2.

Each hand sample was heated to no more than 80 °C and routinely to lower temperatures (~35 to 50 °C) for the samples that are easily dehydrated to deter the loss of structural water and maintain the sulfate coordination. Subsequent to an initial heating, each sample was placed into the sample chamber of the spectrometer and the passively emitted radiation was measured. The *particulate* samples were kept warm by actively heating the sample cups during the data acquisition period of 270 scans at 2 cm^{-1} sampling. The *hand samples* could not be heated actively during the data acquisition, so each of the hand sample spectra was acquired over the shorter course of 160 scans at 2 cm^{-1} sampling to mitigate the effects of sample cooling that produces an unwanted slope in the emissivity spectrum. Each sample was measured on at least three different occasions to co-add the spectra for better signal-to-noise and to produce a representative average spectrum. Additional details of the data calibration are presented in Christensen and Harrison (1993), Wenrich and Christensen (1996), and Ruff et al. (1997).

SPECTRAL RESULTS AND ASSIGNMENT OF THE BANDS

The spectra of solid (nonparticulate), well-crystalline samples are preferred for clearer presentation of the fundamental, diagnostic absorption band positions and representative spectral shape of a mineral. This preference is based upon the relative simplicity of the solid sample spectrum that is free of multiple- and volume-scattering effects that occur in particulate spectra and are magnified with decreasing particle size (e.g., Lyon 1964; Aronson et al. 1966; Hunt and Vincent 1968; Vincent and Hunt 1968; Conel 1969; Hunt and Logan 1972; Aronson and Emslie 1973; Salisbury and Eastes 1985; Moersch 1992; Salisbury and Wald 1992; Wald 1994; Moersch and Christensen 1995; Wald and Salisbury 1995; Mustard and Hays 1997; Lane and Christensen 1998; Lane 1999; Cooper et al. 2002). However, some spectra presented here are of minerals in particulate form, or in poorly consolidated (yet solid) form, because well-crystalline, solid samples were not available. For these spectra, the fundamental absorption bands are shallower, and the bands that result from volume scattering are apparent and may dominate the spectra. Nonetheless, presentation of these spectra is useful, provided the effects of particle size, composition, and hydration state are understood as they correspond to distinct spectral behavior.

Throughout this paper, the sulfate spectra acquired in the laboratory will be presented in groups according to their Strunz classifications (Strunz and Nickel 2001). In each spectral-group figure to be presented, only one spectrum of each mineral from Table 1 is shown (i.e., spectra of duplicate-mineralogy samples are not presented because they are similar to the presented spectra). Each phase produces a distinct spectrum as a result of the fundamental vibrational modes of the crystal structure (Table 2) and their associated overtones and combination bands. Mid-infrared sulfate spectra are dominated by the vibrational behavior of the S-O bonds in the sulfate anion, and in some cases, influenced by the presence of OH or H_2O, or even CO_3, in the structure. Cation complexation of SO_4^{2-} in a solid causes distortions of the sulfate polyhedra (e.g., Griffen and Ribbe 1979) away from simple T_d site symmetry and controls the resulting vibrational spectral features such as band splitting (removal of degeneracy) that results from the

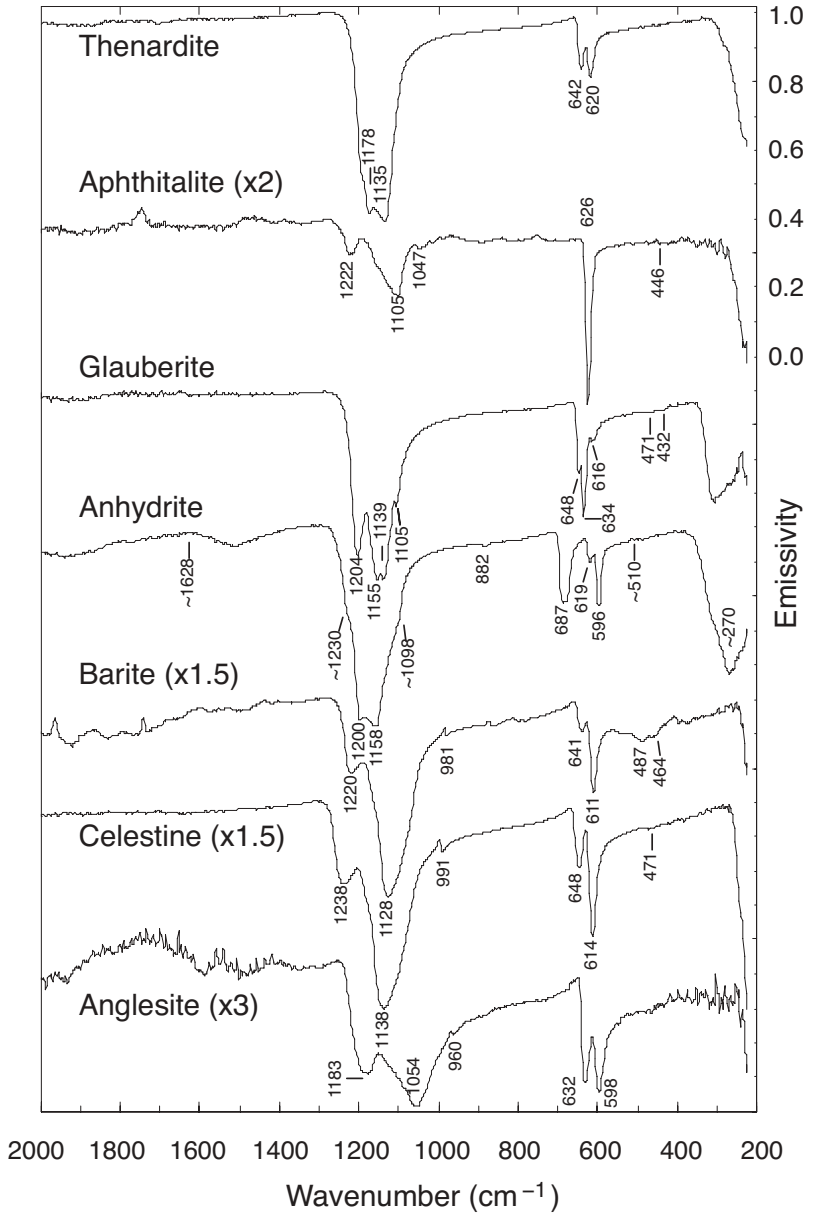

FIGURE 1. Mid-infrared thermal emissivity spectra of anhydrous sulfates. The band depths of some spectra have been modified for easier comparison as noted by the parenthetical values. Spectra are offset for clarity.

lowered symmetry. Although S-O distances vary from mineral to mineral, the grand mean distance is 1.473 [Å (with minimum and maximum distances being 1.430 and 1.501 Å; Hawthorne et al. 2000)]. In a solid-state sulfate, internal vibrational features generally appear at ~1050–1250 (ν_3), ~1000 (ν_1), ~500–700 (ν_4), and ~400–500 (ν_2) cm^{-1} (e.g., Herzberg 1945; Nakamoto 1986; Vassallo and Finnie 1992; Bishop and Murad 2005), and at $\lesssim$550 cm^{-1} due to lattice vibrations (e.g., Serna et al. 1986; Clark 1999) (including metal-oxygen, librational, and translational modes that occur at lower wavenumbers, respectively). The ν_2 band is known to be significantly weaker than the ν_1 mode and commonly is not observable in the infrared spectra of sulfates (Hezel and Ross 1966).

Anhydrous sulfates

The samples of this classification (Strunz 6/A.) presented here include thenardite, aphthitalite, glauberite, anhydrite, celestine, barite, and anglesite. The chemical structure of these sulfates is fairly simple and consists of tetrahedral sulfate groups whose O atoms are coordinated with interstitial cations. The larger the cation, the higher the coordination number (e.g., Ba^{2+} in barite is coordinated with 12 O atoms, the smaller Ca^{2+} in anhydrite is coordinated with eight O atoms, and even smaller Na^{+} in thenardite is coordinated with only six O atoms).

Thenardite, aphthitalite, and glauberite all contain Na^{+} and in the case of aphthitalite and glauberite there is an additional cation of K^{+} and Ca^{2+}, respectively. Thenardite is a structurally simple sulfate whose sulfate polyhedra are closer to T_d symmetry than most other sulfates and whose spectrum is among the simplest (Fig. 1). For thenardite, there is not enough distortion of the sulfate polyhedra to exhibit a ν_1 mode, nor is a ν_2 band seen. The exhibited modes of the sulfate anion shown in emission are ν_3 and ν_4 doublets at 1178/1135 and 642/620 cm^{-1}, respectively, representative of D_{2d} symmetry. However, there is a possible third ν_3 band appearing as a higher-frequency shoulder on the other ν_3 bands, suggestive of a more-distorted D_2 symmetry (Steger and Schmidt 1964, using a transmission technique; Vassallo and Finnie 1992, using an emission technique). The D_2 symmetry determined by Steger and Schmidt (1964) supports a third ν_4 (and ν_3) band that must be degenerate in the emission spectrum shown here because only a doublet is seen. This degeneracy is also the case for the transmission spectra of Moenke (1962) and in one of the two thenardite samples studied in Vassallo and Finnie (1992) (the second thenardite does show a weak third ν_4 band). The band that truncates at 220 cm^{-1} represents a lattice mode vibration. Aphthitalite, also known as glaserite, is unique to the anhydrous sulfate group in that its emission spectrum exhibits only a single, sharp, and very strong vibrational component of the ν_4 band (at 626 cm^{-1}), which also was noted by Moenke (1962) in transmission, whereas the other anhydrous sulfate spectra considered here have at least two and commonly three ν_4 components (Fig. 1). It is likely that in this case, the aphthitalite ν_4 band is doubly degenerate because the sulfate anion in this mineral maintains C_{3v} symmetry (Adler and Kerr 1965), which predicts two ν_4 bands. Two ν_3 bands are present at 1222 and 1105 cm^{-1} and the ν_1 sulfate fundamental vibration appears at 1047 cm^{-1}. There are minor features in the spectrum around 450 cm^{-1}, but it is unclear which minor deviation represents the ν_2 mode [although it may be the small band at 446 cm^{-1} as described in Ross (1974)]. A lattice mode is present but truncated at 220 cm^{-1} (either a metal-O or an SO_4 librational mode). Although a sample of arcanite (K_2SO_4) was not obtained for this study, the spectrum would likely be similar to aphthitalite due to its crystallographic similarities (Washington and Merwin 1921). This prediction appears to be borne out as shown by the transmission spectra of Moenke (1962); however, the aphthitalite spectrum presented by Moenke's shows the ν_3 band to be more widely split than in the arcanite spectrum. The glauberite spectrum (Fig. 1) shows three components of the ν_3 band (at 1204, 1155, and 1139 cm^{-1}), one ν_1 band at 1105 cm^{-1}, three components of the ν_4 band (at 648, 634, and 616 cm^{-1}), and two very weak ν_2 bands (471 and ~432 cm^{-1}) that are difficult to discern in Figure 1. Ross (1974) and Adler and Kerr (1965) proposed either C_2 or C_1 symmetry. The bands presented here would satisfy either C_2 or C_1 symmetry, but cannot further identify which one is correct. The glauberite spectrum also shows the long-wave lattice mode that is present in all the anhydrous sulfates presented in this section.

The only cation in anhydrite is Ca^{2+}. The emissivity spectrum in Figure 1 clearly supports C_{2v} symmetry (e.g., Moenke 1959; Steger and Schmidt 1964; Hezel and Ross 1966, all using transmission data). Figure 1 shows at least two ν_3 bands at 1200 and 1158 cm^{-1} with a possible third band appearing as a shoulder at ~1230 cm^{-1}, and three unequivocal components to the ν_4 band at 687, 619, and 596 cm^{-1}. At ~1098 cm^{-1}, there is a shoulder in the spectrum, likely related to the ν_1 band (Fig. 1), but it is subtle. The ν_1 band of anhydrite is absent in the transmission spectrum presented by Adler and Kerr (1965), but is subtly present in the low-temperature anhydrite emission spectra of Vassallo and Finnie (1992) as a shoulder on a ν_3 band near 1000 cm^{-1}. Ross (1974) and Steger and Schmidt (1964) assign the ν_1 band to 1013 and 1020 cm^{-1}, respectively. More recently, Makreski et al. (2005) assigned a transmission band at 1013 cm^{-1} to ν_1. In the anhydrite spectrum presented here (Fig. 1), there is a distinct small band at 882 cm^{-1} and an emissivity maximum at ~1628 cm^{-1}, both likely due to a minor amount of water being present in the "anhydrous" crystal, resulting from the Ca-OH and H_2O bending motions, respectively. A subtle ν_2 feature occurs at ~510 cm^{-1} (observed at 511 cm^{-1} in Makreski et al. 2005) and a stronger lattice band appears at ~270 cm^{-1}. Comparison of the anhydrite spectrum to spectra of samples of similar composition with different hydration states (e.g., bassanite and gypsum) will be discussed in the "Hydrous sulfates" section.

Overall, because of the relatively large cations associated with the barite group of minerals (barite, celestine, and anglesite), their spectra appear different in shape than the smaller-cation sulfate spectra such as anhydrite that is structurally dissimilar (Fig. 1). The barite-group minerals themselves are isostructural, therefore their spectra are similar to each other, but the Christiansen feature and additional spectral features are offset by small amounts as a result of the different associated cations. The Christiansen feature and the more pronounced spectral features of ν_3 and ν_4, and even the subtler ν_1, are systematically offset to smaller wavenumber (lower energy) for the Sr- (ν_3 = 1238, 1138; ν_4 = 648, 614; ν_1 = 991 cm^{-1}), Ba- (ν_3 = 1220, 1128; ν_4 =641, 611; ν_1 = 981 cm^{-1}), and Pb- (ν_3 = 1183, 1054; ν_4 = 632, 598; ν_1 = 960 cm^{-1}) sulfates, respectively, trending inversely with atomic

weight of the constituent cation. A single ν_2 band is visible for the celestine spectrum at 471 cm^{-1} and ν_2 occurs as a doublet in the barite spectrum at 487 and 464 cm^{-1}, but no ν_2 is obvious for the anglesite spectrum (albeit somewhat noisy). Similarly, the transmission studies of Hezel and Ross (1966) and Wylde et al. (2001) found anglesite (and celestine and barite) not to have a ν_2 band; nor is there an obvious ν_2 band in the anglesite spectrum of Moenke (1962). Here, the ν_3 and ν_4 fundamental sulfate-anion vibrations of the barite-group minerals are shown by two bands each, the ν_1 is non-degenerate (exhibiting only one band), and there is a single ν_2 feature (for celestine), all suggestive of C_{3v} symmetry; however, the transmission studies of Adler and Kerr (1965), Hezel and Ross (1966), and Wylde et al. (2001) showed three ν_3 bands (although the latter study shows only two strong ν_3 bands for celestine with a very weak third ν_3) that would be supportive of a C_s symmetry. Three ν_3 bands also were described for these isostructural minerals by Moenke (1962). The large splitting of the ν_3 bands is related to a large distortion of the sulfate tetrahedron. The band trends presented here for the barite-group minerals are consistent with those discussed in Adler and Kerr (1965) for infrared transmission spectra. However, the extra ν_3 band seen in the transmission data [and a theoretical third ν_4 band and second ν_2 required by C_s symmetry, as identified by Burgio and Clark (2001) for Raman data of barite and as seen here in the barite spectrum] suggest that there may be overlap in the position of the mid-infrared emissivity bands in this isostructural group that would prevent them from being resolved individually. Adler and Kerr (1965) did not discuss the ν_4 band due to their lack of data at the longer wavelengths, but Miller et al. (1960, using transmission data), Moenke (1962), and Wylde et al. (2001) did identify two ν_4 bands, equal to the number identified in this study.

Anhydrous sulfates with additional anions

The samples of this classification (Strunz 6/B.) presented here include antlerite, brochantite, linarite, alunite, minamiite, jarosite, natrojarosite, plumbojarosite, sulfohalite, burkeite, and hanksite. Some of these minerals produce more-complex sulfate spectra due to the presence of hydroxyl (OH) in their structures. Bands can be present in addition to those predicted by the crystal symmetry of the mineral due to hydroxyl groups bonded to one sulfate anion being hydrogen bonded to an adjacent sulfate anion (e.g., Araki 1961; Libowitzky 1999). These additional bands appear predominantly as OH in-plane (δ) and out-of-plane (γ) bending modes. Antlerite and brochantite (both being Cu sulfates) have spectra that are roughly similar (Fig. 2); however, their sulfate anion site symmetries are different [C_s and C_1, respectively, according to Moenke (1962)].

Antlerite, whose crystal structure was well-described by Hawthorne et al. (1989), displays three components of ν_3 (at 1220, 1144, and ~1103 cm^{-1}) and ν_4 (at 670, 639, and 614 cm^{-1}) with an additional feature in the ν_3 range at 1167 cm^{-1} due to OH in the crystal structure (Fig. 2). Antlerite contains four hydroxyls in the unit cell, hence four OH-bending vibrations clearly can be seen at 890, 852, 800, and 756 cm^{-1}. The ν_1 mode is displayed at ~986 cm^{-1}. The ν_2 vibrations occur at 416 and 400 cm^{-1}, consistent with C_s symmetry of the sulfate that predicts two ν_2 bands. The weak 600 and 550 cm^{-1} bands and the strong band at 492 cm^{-1} are assigned to γOH-bending modes. Additional bands at 517, 370, and 334 cm^{-1} can be attributed to Cu-O vibrations. Finally, a band seen as an emissivity maximum at ~1964 cm^{-1} is assigned as the first overtone of the ν_1 vibration (Martens et al. 2003), although that assignment is unproven.

Antlerite forms under pH conditions <4 but if the pH is raised to ~4–6, brochantite will form instead. Ross (1974) defined brochantite to have sulfate anions with C_1 symmetry. This symmetry predicts three ν_3 bands; however, two are shown in Figure 2 at 1132 and 1098 cm^{-1}, but the misshapen former band appears to be two unresolved bands, as is seen more clearly in the brochantite transmission spectrum of Moenke (1962); hence, the shoulder at ~1141 cm^{-1} is assigned to ν_3, as also assigned in the brochantite transmission spectra of Schmidt and Lutz (1993) and Makreski et al. (2005). The ν_1 is displayed at 983 cm^{-1} in agreement with Schmidt and Lutz (1993). Brochantite shows four bands at 938, 875, 848, and 731 cm^{-1} that are attributed to δOH-bending vibrations, and a deep band at 600 cm^{-1} attributed to a γOH-bending vibration. There are many OH lattice vibrational bands that overlie and even interact with the sulfate ν_2 and ν_4 vibrations, making the sulfate and OH band assignments difficult. However, I assign the ν_4 bands of brochantite to the features at ~685, ~648, and ~634 cm^{-1}. Two ν_2 bands are predicted by C_1 symmetry, but no ν_2 bands were assigned from the emissivity spectrum because it is not straightforward to differentiate these modes from Cu-O stretching modes in the same region (Schmidt and Lutz 1993). I have assigned some of the Cu-O stretching bands to the features at 497, 480, 417, and 381 cm^{-1}.

The spectral character of the linarite sample (Fig. 2) is somewhat similar in the ν_3 and ν_4 range to the anhydrous anglesite sample (Fig. 1) that also contains Pb. However, linarite exhibits more ν_3 bands that occur at 1169, 1068, and either the small band at 1050 or 1086 cm^{-1} [comparison to the linarite transmission spectrum of Omori and Kerr (1963) suggests the likelihood of the 1086 cm^{-1} band; however, Moenke (1962) showed the 1050 cm^{-1} band to be the strongest]. Comparison of the linarite spectrum to an emissivity spectrum of cerussite ($PbCO_3$, M.D. Lane, unpublished), a known contaminant in this linarite sample, suggests that the band at 1050 cm^{-1} is due to carbonate contamination, and is not a ν_3 band. The sulfate ν_4 bands occur at 632 and 607 cm^{-1}, but the sulfate symmetry of linarite, that of C_s (Ross 1974), predicts an unseen third ν_4 band. There is another band at 680 cm^{-1}; however, this band clearly is due to the ν_4 of the contaminant carbonate anion. Other bands due to the cerussite are also obvious at 1454 and 1392 cm^{-1} (carbonate ν_3 bands) and at 839 cm^{-1} (carbonate ν_2) (Huang and Kerr 1960). Linarite also shows a sulfate ν_1 at 963 cm^{-1}. Although not apparent in the anhydrous anglesite sample, linarite exhibits two ν_2 bands assigned at 453 and 430 cm^{-1}. There is also a deep band at ~500 cm^{-1} that Ross (1974) attributed to γOH using the transmission data of Moenke (1962). The OH groups in the structure add other spectral bands to linarite that are not seen in the anglesite spectrum. For example, a doublet at 880 and 820 cm^{-1} is due to OH deformation (δ bending) as is the band at 540 cm^{-1} (γ bending). The mode observed at 380 cm^{-1} may be a metal-O vibration.

The mid-infrared features of alunite and/or jarosite and/or varieties thereof are discussed in other works: Shokarev et al. [1972; using transmission (4000–240 cm^{-1})], Powers et al. [1975; using

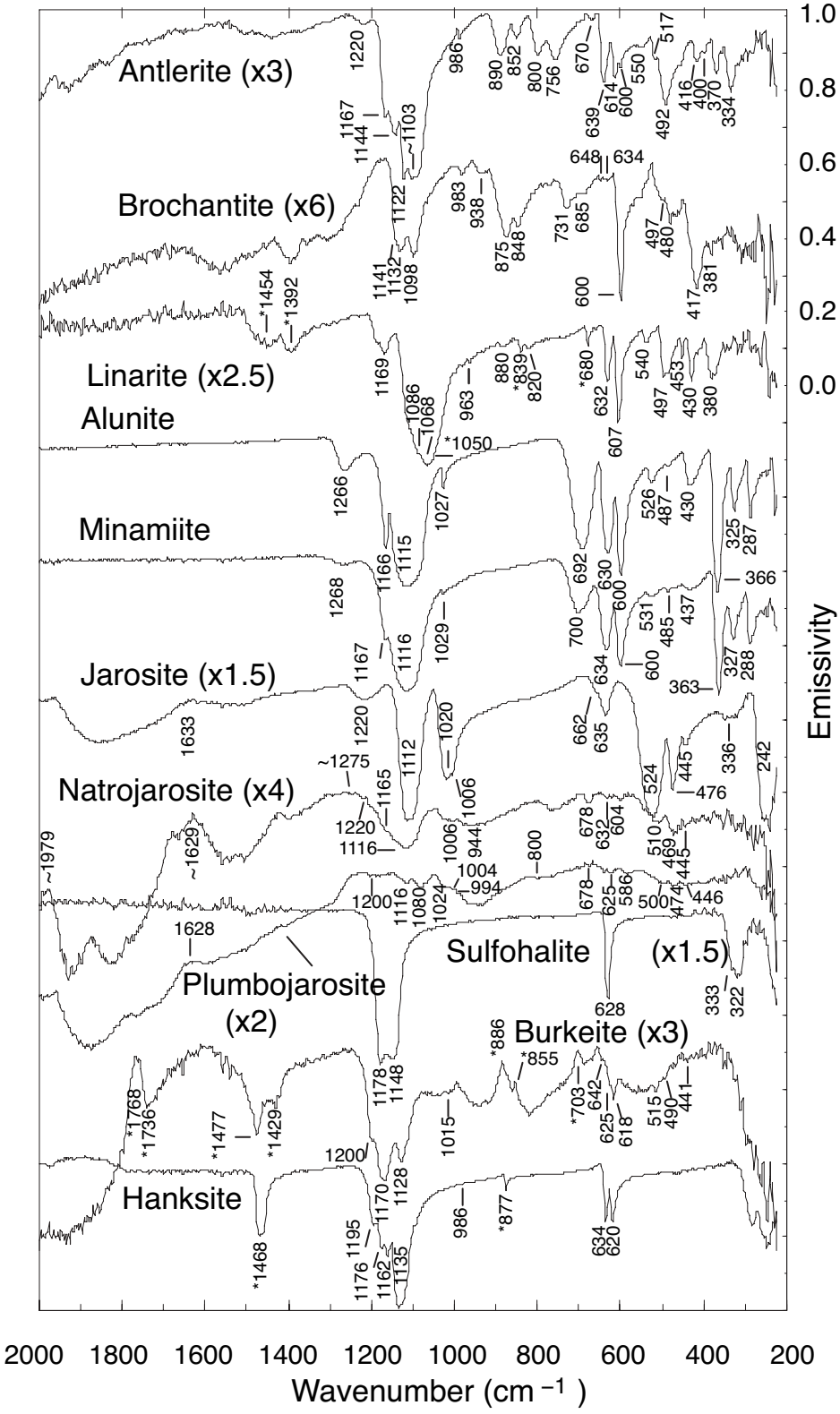

FIGURE 2. Mid-infrared thermal emissivity spectra of anhydrous sulfates with additional anions, where the asterisks denote bands from carbonate contamination (in linarite) or carbonate in the mineral structure. The band depths of some spectra have been modified for easier comparison as noted by the parenthetical values. Spectra are offset for clarity.

transmission (4000–200 cm^{-1})], Serna et al. [1986; using Raman (3700–50 cm^{-1}) and transmission (4000–100 cm^{-1})], Breitinger et al. [1997; using Raman (<1500 cm^{-1}) and transmission (3600–400 cm^{-1})], Sasaki et al. [1998; using Raman (1300–200 cm^{-1}) and diffuse reflectance (4000–400 cm^{-1})], Sejkora and Ďuda [1998; using transmission (4000–400 cm^{-1})], and Bishop and Murad [2005; using reflectance (~33 000–200 cm^{-1}) and transmssion (4000–400 cm^{-1})]. The emissivity spectra presented here of alunite and jarosite (Fig. 2) are different in shape from their transmittance and reflectance counterparts, but exhibit many of the same spectral features.

Alunite displays two ν_3 features at 1266 and 1115 cm^{-1}. The ν_1 feature occurs at 1027 cm^{-1} as supported by the study of Serna et al. (1986) and Breitinger et al. (1997), the two ν_4 bands occur at 692 and 630 cm^{-1}, and a single ν_2 band occurs at 430 cm^{-1}. The observation of these bands supports C_{3v} symmetry of the sulfate tetrahedron. A sharp band at 1166 cm^{-1} is due to δOH, so identified because deuteration greatly shifts this band to lower frequency (Breitinger et al. 1997). Breitinger et al. also demonstrated that this δOH band undergoes a Fermi resonance with the 1115-cm^{-1} ν_3 band. Additional bands are exhibited at: 600 cm^{-1} (due to γOH), and 526 and 487 cm^{-1} (both due to Al-O). Bands at 366, 325, and 287 cm^{-1} have been attributed to Al-O bonds for the octahedral structural components (Serna et al. 1986).

The minamiite spectrum (Fig. 2) is virtually identical to that of alunite. Because they are from the same crystal system (i.e., trigonal-rhombohedral), their spectra should be quite similar; however, the cations Na^+ and Ca^{2+} in the minamiite

TABLE 2. Band assignments of the fundamental vibrational modes in sulfate-bearing minerals (in cm^{-1})

Mineral	δH_2O	ν_3	δOH	ν_1	H_2O libration	δOH	ν_4	γOH	ν_2	H_2O libration	M-O or lattice
Afghanite†		1171					609				434
		1128					590				
		1022					540?				
Alunite		1266									
		1115	1166	1027			692	600	430		526
							630				487
											366
											325
											287
Anglesite		1183		960			632				
		1054					598				trunc.
Anhydrite	~1628	1200		~1098? (sh)		882	687		510		270
		1158					619				
		~1230?					596				
Antlerite		1220	1167	~986		890	670	600	416		517
		1144				852	639	550	400		370
		~1103				800	614	492			334
						756					
Aphthitalite		1222		1047			626		446?		trunc.
		1105									
Apjohnite	~1690	1115		992		944	705				trunc.
		1080					640				
		1054					580				
Barite		1220									
		1128		981			641		487		trunc.
							611		464		
Bassanite	1630	1171		1000			664				~240
		1158					630				
		1093					600				
Bloedite		~1190 (sh)		992		820	~653 (sh)		469		310
		1158				719	634 (sh)		428		trunc.
		1121					614				
Brochantite		~1141 (sh)		983		938	~685	600			497 (sh)
		1132				875	~648				480
		1098				848	~634				417
						731					381
											~297
Burkeite‡		1200 (sh)		1015		~625 (sh)			441?		515?
		1170				~642 (sh)					490? (sh)
		1128				618					trunc.
Celestine		1238		991			648		471		trunc.
		1138					614				
Coquimbite		1180									
		1100		1013		890	685		480		278
						816	650		443		
							597				
Creedite		1180		983		806	676		497		386
		1154				772	640		478		trunc.
		1098					570				
		1043									
Ferricopiapite	1649	1220		997			600		~467		trunc.
	1444	~1116					552				
		~1050									
Glauberite		1204		1105			648		471		308
		1155					634		~432		
		1139					616				
Gypsum	1621	1155		1010*		877*	676			475	trunc.
							604				
							595? (sh)				
Hanksite§		1195		986			634				285
		1176					620				249
		1162									
		1135									
"Hexahydrite"		1254		1045	917		676		462?		409
(likely kieserite)		1222 (sh)					643				375
		1180					614				358
											322
											trunc.

Notes: (sh) = Band occurs as a shoulder on a larger band; trunc. = Band is truncated, so band minimum is not known.

* Band location is identifiable only because of Type III band behavior (Hunt and Vincent, 1968) in a fine-grained (<10 μm) sample.

† Afghanite exhibits additional vibrational modes due to carbonate anions in the mineral structure (~1560–1387 cm^{-1}, ν_3; 887 cm^{-1}, ν_2; 735 cm^{-1}, ν_4; ~400–250 cm^{-1}, lattice mode) and Si-Al-O bending modes at 682 and 662 cm^{-1}.

‡ Burkeite exhibits additional vibrational modes due to carbonate anions in the mineral structure (1477 and 1429cm^{-1}, ν_3; 886 cm^{-1}, ν_2; 703 cm^{-1}, ν_4).

§ Hanksite exhibits additional vibrational modes due to carbonate anions in the mineral structure (1468 cm^{-1}, ν_3; 877 cm^{-1}).

|| Thaumasite exhibits additional vibrational modes due to carbonate anions in the mineral structure (1392 cm^{-1}, ν_3; 880 cm^{-1}, ν_2; 329 cm^{-1}, lattice mode) and Si-O (765 and 680 cm^{-1}, νSi-O; 494 and ~460 cm^{-1}, δSi-O).

Linarite contains contaminant cerussite and hence has observable carbonate bands at 1454, 1392, 1050, 839, and 680 cm^{-1}.

TABLE 2.—*Continued*

Mineral	δH_2O	ν_3	δOH	ν_1	H_2O libration	δOH	ν_4	γOH	ν_2	H_2O libration	M-O or lattice
Jarosite	1633	1220	1020	1006			~662 (sh)		445		524
		1112					635				476
											~336
											~242
Kainite	1654	1181			1020	809	660		468		285
		1135				744	643		441?		
		1128					602				
Kieserite		1256		1045	919		669		458?		~352
		~1213 (sh)					641				
		1183					~610				
Linarite#		1169		963		880	632	540	453		380
		1086 (sh)				820	607	497	430		
		1068									
Minamiite		1268	1167	1029			700	600	437		531
		1116					634				485
											363
											327
											288
Natrojarosite	1629	1220	~1010 (sh)	~1006			678	604	445		510
		~1165 (sh)					~632				469
		1116									trunc.
Pickeringite	~1680	1115		985		~945	~705		480		trunc.
		1080					~646 (sh)				
		1047					~588	586	446		50
Plumbojarosite	~1628	1200	1024	1004?			~678				474
		1116					~6250				trunc.
		1080									
Polyhalite	1651	~1231 (sh)		~1010	744		657		471?		244
		1192		988	687		623				
		1172					602				
		1102									
Potassium Alum	~1690	1226 (sh)		993			~653		~443?		trunc.
		1128					593				
		1055									
Rozenite	~1680	~1220 (sh)		992		818	~660 (sh)		468?		
		1100				~760	~645 (sh)				
		~1013				735	602		~467		384
						~692	641				
Serpierite	~1665	1144		983		825	600				
		1123				~687					
		1098									
Sulfohalite		1178					628				333 (sh)
		1148									
		322									
Szomolnokite		1226 (sh)		1018	846		626		361?		trunc.
		1195					606				
		1149					554				
Thaumasite||	1712	~1135 (sh)		999			636				trunc.
		1095					588				
		1066 (sh)					642				trunc.
Thenardite§		1178					620				
		1135									
Zincobotryogen	1660	1220	1010?	999		806?	602		393?		280
		1164 (sh)					545				
		1132					485				
		1068									
		1031									

Notes: (sh) = Band occurs as a shoulder on a larger band; trunc. = Band is truncated, so band minimum is not known.
* Band location is identifiable only because of Type III band behavior (Hunt and Vincent, 1968) in a fine-grained (<10 μm) sample.
† Afghanite exhibits additional vibrational modes due to carbonate anions in the mineral structure (~1560–1387 cm^{-1}, ν_3; 887 cm^{-1}, ν_2; 735 cm^{-1}, ν_4; ~400–250 cm^{-1}, lattice mode) and Si-Al-O bending modes at 682 and 662 cm^{-1}.
‡ Burkeite exhibits additional vibrational modes due to carbonate anions in the mineral structure (1477 and 1429cm^{-1}, ν_3; 886 cm^{-1}, ν_2; 703 cm^{-1}, ν_4).
§ Hanksite exhibits additional vibrational modes due to carbonate anions in the mineral structure (1468 cm^{-1}, ν_3; 877 cm^{-1}).
|| Thaumasite exhibits additional vibrational modes due to carbonate anions in the mineral structure (1392 cm^{-1}, ν_3; 880 cm^{-1}, ν_2; 329 cm^{-1}, lattice mode) and Si-O (765 and 680 cm^{-1}, νSi-O; 494 and ~460 cm^{-1}, δSi-O).
Linarite contains contaminant cerussite and hence has observable carbonate bands at 1454, 1392, 1050, 839, and 680 cm^{-1}.

have a smaller radius than K^+, hence the minamiite spectral features likely should be offset to higher wavenumbers (higher frequency) due to the stronger bonds. The bands are shifted minimally and may be due partially to the impurity of the minamiite, which is contaminated by ~8% alunite. The largest shifts, albeit small, are seen in the position of the ν_4 bands. For minamiite, they are located at 700 and 634 cm^{-1}. The depths of some of the minamiite features are shallower relative to the same bands in alunite (i.e., the bands at 1268, 1167, 1029, 700, 531, and 437 cm^{-1}). These band-depth differences likely are crystal-axis orientation effects.

Jarosite, natrojarosite, and plumbojarosite are all also isostructural to alunite. Jarosite exhibits two ν_3 bands at 1220 and 1112 cm^{-1}, a ν_1 band at 1006 cm^{-1}, and a single ν_2 at 445 cm^{-1}. The

jarosite spectrum shows a subtle shoulder at ~662 on a stronger feature at 635 cm^{-1} suggesting two ν_4 bands [as also was seen in the transmission spectra of Powers et al. (1975), Serna et al. (1986), and Bishop and Murad (2005)]. These bands suggest C_{3v} sulfate symmetry as supported by other studies (e.g., Adler and Kerr 1965; Ross 1974; Lazaroff et al. 1982). Additional modes of jarosite are shown to occur at ~1020 (due to δOH) and 524, 476, ~336, and ~242 cm^{-1} due to Fe-O lattice modes. Shokarev et al. (1972) and Lazaroff et al. (1982) assigned the former two bands to τOH-translational modes and the band at ~336 cm^{-1} to a τSO_4-translational mode using their transmission spectra. The broader lattice-mode band at 524 cm^{-1} suggests a possible superposed γOH mode on the higher frequency side of the feature as observed by both Serna et al. (1986) and Sasaki et al. (1998). An emissivity maximum at 1633 cm^{-1} results from δH_2O. Jarosites and alunites are isostructural, but the sulfate tetrahedra are more distorted in alunite, hence the split between the ν_3 modes is ~151 cm^{-1} in alunite and 108 cm^{-1} in jarosite. This relationship of the ν_3 bands is similar to that noted by Serna et al. (1986).

Natrojarosite differs from jarosite through the replacement of K^+ by Na^+ in the structure. Theoretically, natrojarosite should exhibit the same features as jarosite but with bands shifted to higher frequencies as a result of the smaller cation (Na^+) in the structure. Inspection of Figure 2 shows otherwise, primarily because the natrojarosite spectrum exhibits features that result from scattering in a particulate sample. For example, the decreased emissivity at ≳1275 cm^{-1} and the broad, bowl-shaped feature with an emissivity minimum at ~944 cm^{-1} result from the finer effective particle size of the natrojarosite. The natrojarosite spectrum does, however, display a ν_3 feature at ~1116 cm^{-1} that occurs at a slightly higher wavenumber than the jarosite counterpart. This relationship also was seen by Sasaki et al. (1998) and Bishop and Murad (2005). A second ν_3 feature is not distinct, but may be a small feature at (~1220 cm^{-1}). The former ν_3 feature is broadened on the higher-frequency side likely due to another ν_3 band that is apparent at ~1165 cm^{-1}. Three ν_3 features were identified in Sasaki et al. (1998) likely due to the presence of both Na and Fe cations, even though the C_{3v} sulfate symmetry predicts only two ν_3 features. The feature at ~1006 cm^{-1} is the ν_1 band, but its higher-frequency breadth is due to a superposed δOH band. The ν_4 feature of natrojarosite occurs at 678 cm^{-1}. Although not as clear as the previous band, another ν_4 feature occurs at ~632 cm^{-1}. These ν_4 bands of natrojarosite show broader splitting than in jarosite. The ν_2 band is assigned at 445 cm^{-1} (just as in jarosite), and other bands occur at 604 cm^{-1} (due to γOH), and at 510 and 469 cm^{-1} [due to Fe-O vibrations; Shokarev et al. (1972) and Lazaroff et al. (1982) assign these two bands to τOH-translational modes]. An emissivity maximum at 1629 cm^{-1} is due to the bending vibration of water (δH_2O) (e.g., Sejkora and Ďuda 1998, using transmission data). The emissivity maximum at ~1979 cm^{-1} is thought to be the overtone of the δOH feature (Bishop and Murad 2005) that occurs at ~1010 cm^{-1}; however, Bishop and Murad (2005) also suggest that this band could be the overtone of a ν_3 band, but that assignment does not seem to fit the emissivity data as well as the δOH overtone assignment. Future deuteration studies could verify the proper assignment. Other features that arise from combinations and overtones occur, but have not been assigned.

The plumbojarosite sample is a particulate sample, hence its spectrum shows evidence of volume scattering. Volume scattering is manifested as broad emissivity minima at >1240 cm^{-1} and ~1050 to 820 cm^{-1}. Sasaki et al. (1998) noted that the Pb^{2+} cations occupy only half of the sites of K^+ in jarosite and Na^+ in natrojarosite (i.e., in a unit structure there is an SO_4^{2-} adjacent to Pb^{2+} ions and an SO_4^{2-} adjacent to vacant sites); a related difference is that the crystallographic unit-cell **c** parameter (33.85 Å) is about twice that of jarosite and natrojarosite (17.22 and 16.72 Å, respectively). Sasaki et al. (1998) found that the **c** parameter affects the stretching modes (ν_1 and ν_3) but not the bending modes (ν_2 and ν_4). This causality allows plumbojarosite to exhibit three ν_3 bands—at 1200, 1116, and 1080 cm^{-1}—when only two ν_3 bands are predicted for the sulfate symmetry. Three ν_3 bands are consistent with the number observed by Sasaki et al. (1998). It is unclear where the ν_1 mode appears; it could be either [or both due to the peculiar unit structure of plumbojarosite mentioned above and seen in Sasaki et al. (1998)] of the two shoulders at 1004 and 994 cm^{-1} on the deeper volume-scattering feature. Between the possible ν_1 and the ν_3 bands lies a feature at 1024 cm^{-1} due to δOH. The ν_4 bands appear at ~678 and ~625 cm^{-1} (the inflection within this second band is thought to be noise in the spectrum) and the ν_2 band occurs at 446 cm^{-1}. Other bands include an emissivity maximum at ~1628 cm^{-1} due to the bending vibration of water (δH_2O) (e.g., Omori and Kerr 1963), an unidentified band at 800 cm^{-1} [similar in position to an unassigned band in natrojarosite in the transmission spectrum of Bishop and Murad (2005)], a γOH band at 586 cm^{-1}, and bands at 500 and 474 cm^{-1} due to Fe-O vibrations.

The other sulfates in this class exhibit simpler spectra regardless the presence of being another anion in the structure such as F and Cl in sulfohalite, CO_3 in burkeite, and CO_3 and Cl in hanksite (Fig. 2). The spectrum of isometric sulfohalite, whose structure is composed of sulfate anions surrounded by 12 Na cations as well as NaF and NaCl octahedra, exhibits traditional features related to the internal vibrations of the sulfate anion. The ν_3 doublet features occur at 1178 and 1148 cm^{-1} and a ν_4 singlet occurs at 628 cm^{-1}. This isometric crystal exhibits no apparent ν_1 or ν_2 bands, suggestive of a fairly undeformed sulfate tetrahedron; the lack of ν_1 and ν_2 plus the two ν_3 bands suggest D_{2d} symmetry. This symmetry permits two ν_4 bands but only one is visible, hence the ν_4 band must be doubly degenerate. However, Omori (1970) suggested T_d symmetry for the sulfate anions in sulfohalite. By using factor group analysis (on the space group O_h^5 and site group T_d of the SO_4 ion) and the calculated force constants of the Urey-Bradley force field (Urey and Bradley 1931), Omori calculated the normal modes of vibration of sulfohalite that he attributes to combination bands of the lattice modes in the far infrared. His mathematical determinations match well the bands in his transmission spectrum which is similar to the measured emissivity spectrum of sulfohalite (Fig. 2) and predict the splitting seen in the ν_3 bands, due to combinations of the SO_4 molecular vibrations and long-wavelength lattice modes [i.e., internal-external combination bands (Mitra 1963)]. The deep bands that occur superposed at ~333 and 322 cm^{-1} were attributed by Omori (1970) to lattice vibrations that arise from the Na_6Cl and Na_6F octahedra. Another lattice-mode band is present, but truncated at 220 cm^{-1}.

Although White (1974) stated that "…detailed interpretation is impossible" (p. 273) of spectra of minerals with complex structures, including burkeite, I disagree with that view and my interpretation follows. The burkeite spectrum (Fig. 2) clearly shows spectral evidence of both the SO_4 and CO_3 anions. The spectral character at >1250 cm^{-1} is dominated by the behavior of the carbonate anion (e.g., the emissivity maximum at 1768 cm^{-1} and the neighboring band at 1736 cm^{-1}; the emissivity minimum at 1477 and 1429 cm^{-1} due to CO_3 ν_3). Carbonate also causes the emissivity maxima at 886 cm^{-1} (CO_3 ν_2), 855, and 703 cm^{-1} (CO_3 ν_4) (Lane and Christensen 1997). These are maxima because they are transparency features [Type II and Type III behaviors, as classified by Hunt and Vincent (1968)] related to the friable nature of the sample that has a fine powder on the surface. A fine-grained spectrum of carbonate can be seen in Lane (1999) for comparison and for detailed discussion of the similar spectral features. The sulfate anion in burkeite causes features at 1200, 1170, and 1128 cm^{-1} all related to the sulfate ν_3 asymmetric-stretching vibration. The weak emissivity minimum at 1015 cm^{-1} is due to the sulfate ν_1 and the band at 618 cm^{-1} is due to ν_4, and it is likely that the shoulders at 642 and 625 cm^{-1} are also likely ν_4 features. These bands suggest the possibility of C_{2v}, C_2, C_s, or C_1 symmetry of the sulfate, but it is not clear which one is correct. All of these possibilities predict one to two ν_2 bands; however, it is not clear which of the spectral feature(s) represent this mode; perhaps it is the band at 441 cm^{-1}. The bands at 515 and 490 cm^{-1} possibly are due to metal-O bonds. Finally, burkeite exhibits a very strong feature truncated at 220 cm^{-1}, representing a lattice mode.

Hanksite also contains features related to constituent carbonate. These carbonate bands occur at 1468 and 877 (ν_3 and ν_2, respectively). Omori and Kerr (1963) also noted these carbonate bands in their hanksite transmission spectrum. There are four sulfate ν_3 bands at 1195, 1176, 1162, and 1135 cm^{-1} due to both K and Na being bound to the sulfate anions. The sulfate ν_1 band appears as a subtle feature at 986 cm^{-1}. Two strong bands at 634 and 620 cm^{-1} represent the sulfate ν_4 mode. The lower-wavenumber bands at 285 and 249 cm^{-1} are lattice modes.

Hydrous sulfates

The samples of this classification (Strunz 6/C.) presented here include kieserite, szomolnokite, rozenite, hexahydrite, coquimbite/paracoquimbite, pickeringite, apjohnite, potassium alum, bloedite, polyhalite, bassanite, and gypsum. For this subclass, each mineral contains bound H_2O, in various abundances. It should be noted that this study did not extend to the higher frequencies at which bound water is best studied due to the presence of the strong OH-stretching modes (~4000–3000 cm^{-1}) and at even higher frequencies due to water overtones (~6500–7000 cm^{-1}). However, continued research with the samples studied in this work is being conducted with other spectroscopic techniques (e.g., Lane et al. 2004), including the higher frequency region.

A kieserite spectrum is shown in Figure 3. The sulfate ν_3 bands in this monohydrate are present at 1256 and 1183 cm^{-1} with a subtle third band at ~1213 cm^{-1}. The ν_1 band is seen at 1045 cm^{-1} and three ν_4 bands occur at 669, 641, and ~610 cm^{-1}. The feature at 458 cm^{-1} is assigned to the ν_2 band. The sulfate tetrahedra in kieserite are known to be in C_2 site symmetry (e.g., Hezel and Ross 1966; Stoilova and Lutz 2002). This symmetry predicts the three ν_3 and ν_4 bands and a single ν_1 band, but also an additional ν_2 band that is unassigned here. There is a pronounced feature at 919 cm^{-1} that is uncommon but otherwise is seen only in szomolnokite (also a monohydrated Fe-sulfate) of the other sulfates in this paper. This uncommon band likely is due to the unusual librational modes of the water molecule seen in kieserite-group minerals but not in other hydrates in which water molecules form a similar coordination (Grodzicki and Piszczek 1998). The presence of this band is a reliable indicator of monohydrated kieserite-group sulfates. This water libration band also appears very distinctly in the kieserite transmission spectrum of Moenke (1962). The long-wave, broad band at ~350 cm^{-1} is due likely to the M-O vibration in the coordinated sulfate anion (Ferraro and Walker 1965).

Szomolnokite also is a monohydrated sulfate and it is considered to be an end-member in a solid-solution series with kieserite (Jambor et al. 2000). The szomolnokite hand sample is well-crystalline and provided strong spectral features (Fig. 3). This szomolnokite spectrum closely resembles that of kieserite; however, the szomolnokite spectral features are shifted to longer wavelengths by roughly 20–100 wavenumbers. The internal vibrational bands due to the sulfate anion are distinct in the spectrum shown in Figure 3 and consist of three ν_3 bands at 1226, 1195, and 1149 cm^{-1}. The ν_1 band appears as a small feature at 1018 cm^{-1}. Features at 626, 606, and 554 cm^{-1} result from the ν_4 vibrations. The unusual emission feature at 846 cm^{-1} is due to water libration (Grodzicki and Piszczek 1998), as was seen in the kieserite spectrum at 919 cm^{-1}. The sharp feature at ~669 cm^{-1} is due to the improper removal of atmospheric CO_2 in the sample chamber and is not related to the mineral sample itself. The many sulfate-related absorption features result from the distortions of the SO_4 tetrahedron, and the number of bands supports the C_2 site symmetry for sulfate anion in szomolnokite, a kieserite-group mineral (Hezel and Ross 1966). This symmetry additionally predicts two ν_2 bands, one of which could be represented by the feature at 361 cm^{-1} but the assignment is uncertain. The truncated band at ~275 likely is due to a Fe-O vibration.

The mineral rozenite is closely related to szomolnokite because the former is known to dehydrate readily to the latter. The water in rozenite causes an emissivity maximum at ~1680 cm^{-1} (due to the δH_2O mode), a band at 818 cm^{-1}, and weaker bands at ~760, 735, and 692 cm^{-1} that likely result from δOH (Fig. 3). Rozenite exhibits a deep ν_3 feature at 1100 cm^{-1} and two small shoulder features at ~1013 and 1195–1260 cm^{-1} that also are representative of the ν_3 bands. The ν_1 band appears at 992 cm^{-1}. The rozenite spectrum shows a fairly broad ν_4 band centered at ~602 cm^{-1} with two other ν_4 bands that appear as subtle shoulders on the higher frequency side at ~660 and 645 cm^{-1}, and a possible ν_2 band at 468 cm^{-1}. The emissivity bands present in the monoclinic rozenite spectrum cannot identify further the sulfate site symmetry beyond either C_1 or C_2.

The hexahydrite spectrum shown in Figure 3 appears almost identical to the kieserite spectrum also shown in that figure and discussed above. Both spectra exhibit the uncommon feature at ~920 cm^{-1} thought to be unique to and diagnostic of the monohydrated, kieserite-group sulfates (Grodzicki and Piszczek 1998), as is seen also in the spectrum of monohydrated szomolnokite discussed above. Kieserite readily hydrates to hexahydrite

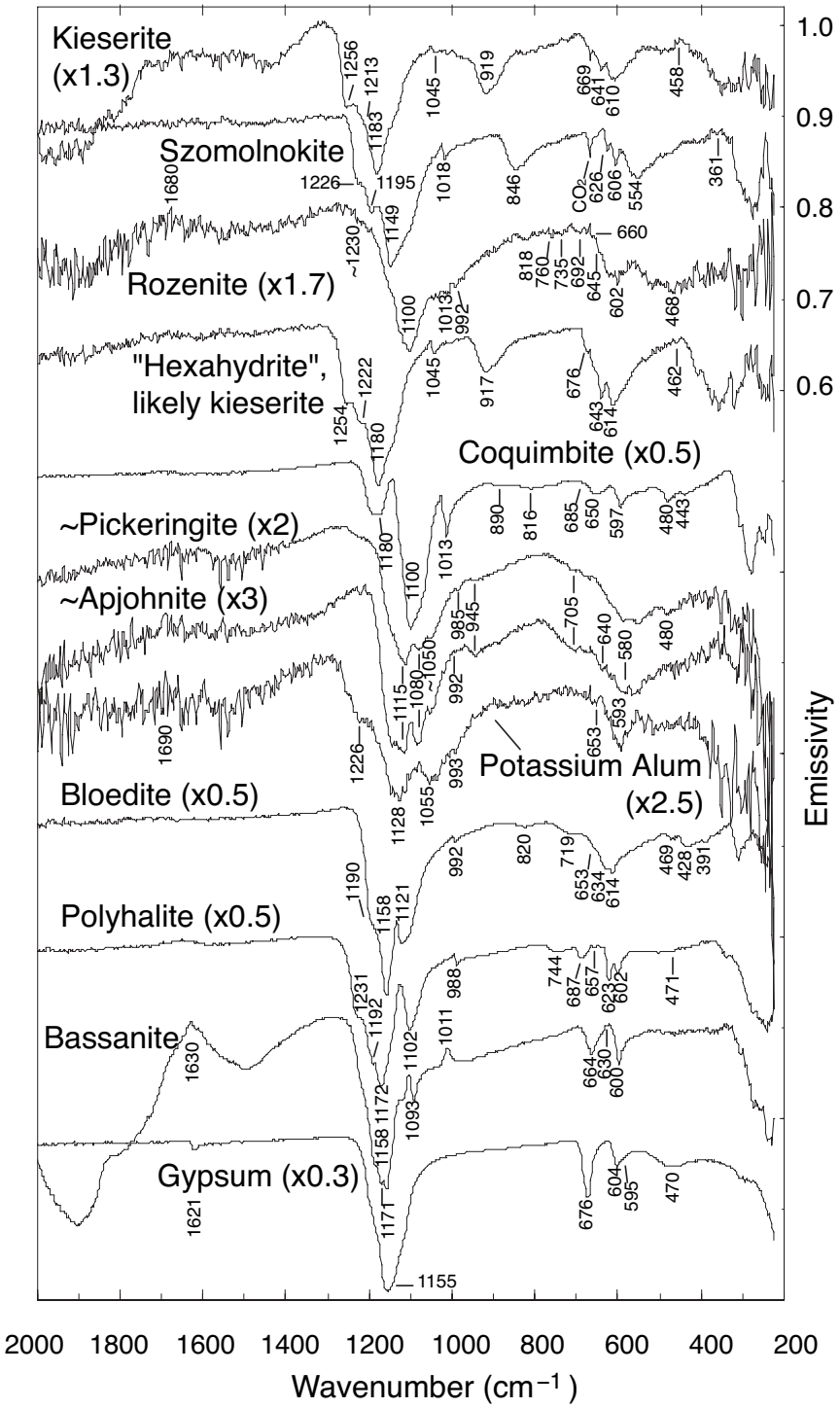

FIGURE 3. Mid-infrared thermal emissivity spectra of hydrous sulfates. The band depths of some spectra have been modified for easier comparison as noted by the parenthetical values. Spectra are offset for clarity.

(Vaniman et al. 2004), so it would seem likely that these spectra could be of the same species (i.e., kieserite); however, XRD measurements were made on the samples and their phases were deemed correct. Nonetheless, it is the opinion of the author that the "hexahydrite" spectrum is actually that of kieserite and that the sample hydrated between the emission measurement and the XRD measurement. Future work will have to revisit the hydration/dehydration trends of the Mg sulfates, and better assessment/control of their hydration must be done to understand fully the spectral differences between the mineral species. On the basis of the "hexahydrite" spectrum shown, the bands occur as follows: three ν_3 at 1254, 1222, and 1180 cm^{-1}; ν_1 at 1045 cm^{-1}; water libration at 917 cm^{-1}; ν_4 at 676, 643, and 614 cm^{-1} and ν_2 possibly at 462 cm^{-1}; however, these likely are the appropriate band assignments for kieserite, not actual hexahydrite. The long-wave, broad band at ~358 cm^{-1} and its neighboring inflections are due likely to M-O vibrations in the coordinated sulfate anion (Ferraro and Walker 1965).

The coquimbite/paracoquimbite sample is well-crystalline and contains approximately subequal amounts of the two minerals, which are polytypic. The coquimbite/paracoquimbite spectrum (Fig. 3) shows two clear ν_3 features at 1180 and 1100 cm^{-1}; the shape of the 1100 cm^{-1} band suggests that there may be another weaker ν_3 band at slightly lower frequency [three bands were seen in transmission data of Moenke, (1962) as reported by Ross (1974)]. A strong ν_1 feature is present at 1013 cm^{-1}. Three ν_4 bands occur at 685, 650, and 597 cm^{-1}; however, the 685 cm^{-1} band is very small, but distinct in this very clean spectrum. The ν_2 features occur at 480 and 443 cm^{-1} with strong lattice modes occurring at <350 cm^{-1}. The bands that result from the water in the coquimbite structure can be seen at ~890 and 816 cm^{-1} (bending modes).

Neither the pickeringite nor apjohnite samples are pure, as determined by XRD analyses; each sample contains both of the above plus subordinate amounts of kalinite and halotrichite [$FeAl_2(SO_4)_4 \cdot 22H_2O$]. These mineral assemblages are quite common due to the extensive solid solution between them and that they are all halotrichite-group minerals (Jambor et al. 2000), except for kalinite. For this reason these two spectra are very similar and discussed together. These spectra each show three ν_3 bands at ~1115, ~1080, and 1047–1054 cm^{-1}. Two ν_3

bands for pickeringite in Ross (1974) are listed as occurring at 1085 and 1025 cm^{-1}; however, the latter is a carryover typo from Moenke (1962), which still is being propagated incorrectly in the literature (e.g., see Frost et al. 2000, 2005) and actually is seen clearly in the Moenke spectrum at 1125 cm^{-1}. Although only two ν_3 bands were identified from Moenke (1962), the Moenke pickeringite spectrum very closely resembles the Moenke halotrichite spectrum in which a subtle band at ~1068 cm^{-1} also was identified as a ν_3 band (Ross 1974). Considering the similarity between the Moenke pickeringite and halotrichite spectra and of the "pickeringite" and "apjohnite" spectra of this study, and the fact that they are all halotrichite-group minerals, the band assignments I give to the ν_3 bands are supported. A ν_1 band is seen at 985 cm^{-1} (this band is subtle in the "apjohnite" spectrum and occurs at 992 cm^{-1}). A clearer band occurs at ~945 cm^{-1} in both spectra that likely is due to the bending mode of the OH in the structures. The bending mode of H_2O appears as an emissivity maximum at ~1680 cm^{-1} (Ross 1974). The ν_4 bands can be seen at ~705, 640, and 580 cm^{-1}, but these bands are fairly ill-defined, likely as a result of extensive solid solution and the impurities of the minerals. A band in "pickeringite" occurs at ~480 cm^{-1} that likely is due to a ν_2 mode [a band at 480 cm^{-1} in the halotrichite spectrum of Moenke (1962) also was identified as ν_2]; however, no additional ν_2 band is obvious [but is predicted by either C_1 or C_2 site symmetry (Ross 1974)]; nor are any clear ν_2 bands seen in the "apjohnite" spectrum. These spectra are fairly noisy though, due to keeping the sample temperatures low during measurement to prevent water from being driven out of the samples.

Due to low temperatures during data acquisition, the potassium alum (that is, potash alum or kalinite) spectrum (Fig. 3) is also a bit noisy. However, three ν_3 bands are seen at 1226, 1128, and 1055 cm^{-1}, whereas the ν_1 band is seen at 993 cm^{-1}. A pronounced ν_4 feature occurs at ~593 cm^{-1} and a second likely ν_4 band occurs at ~653 cm^{-1}, but a third ν_4 band was not assigned, even though it is predicted by what appears to be C_{2v} sulfate symmetry on the basis of the other bands presented here. This symmetry determination is consistent with the results of Frost and Kloprogge (2001) but is inconsistent with the C_{3v} symmetry of Campbell et al. (1970) and Ross (1974) that would only allow two ν_3 bands. However, the Moenke (1962) transmission data that Ross interpreted as having only two ν_3 bands does indeed show a band at 1075 cm^{-1} that I interpret as a third ν_3 band (disallowed by C_{3v} symmetry), reinforcing my interpretation of C_{2v} sulfate symmetry in potassium alum. A vibrational band related to the water bending mode is seen as a subtle emissivity maximum at ~1690 cm^{-1} (Frost et al. 2000), and the general absorption at ~500 cm^{-1} may be due to a water libration mode and a superposed ν_2, although these individual bands are not distinct in this spectrum.

The bloedite spectrum (Fig. 3) exhibits three ν_3 bands at 1190 (shoulder), 1158, and 1121 cm^{-1}, and a ν_1 band at 992 cm^{-1}. The ν_4 bands were assigned at 653 (shoulder), 634, and 614 cm^{-1} and two ν_2 bands are seen at 469 and 428 cm^{-1}. These band assignments are consistent with C_1 sulfate symmetry (Ross 1974). The bands seen at 820 and 719 cm^{-1} are due to the water-bending modes present in the mineral. The features at 391 cm^{-1} and lower frequency likely are lattice modes.

Polyhalite (Fig. 3) exhibits ν_3 features at 1231 (shoulder), 1172, and 1102 cm^{-1}; an additional small band at 1192 cm^{-1} is also likely a ν_3 mode associated with another of the three cations in the mineral (K, Mg, Ca) that also are coordinated to the sulfate anion and offer various sulfate polyhedral distortions. A sharp ν_1 feature occurs at 988 cm^{-1} with an additional small ν_1 band at 1010 cm^{-1} due to the many sulfate distortions. The ν_4 bands occur at 623 and 602 with a small third band at 657 cm^{-1}. The 744 and 687 cm^{-1} bands are water librational modes (Ross 1974; Gadsden 1975). The emissivity maximum at 1651 cm^{-1} is the manifestation of the H_2O-bending mode (e.g., Omori and Kerr 1963; Ross 1974). The ν_2 bands are small enough not to be able to assign properly; however, the symmetry of the sulfate anion (C_1, Ross 1974) predicts two bands, one of which may be the band at ~471 cm^{-1}. The band at ~244 cm^{-1} that is truncated at longer wavelengths is interpreted as a lattice mode. The emissivity spectrum presented here appears with fewer bands than the "very complex" transmission spectrum of Moenke (1962) described by Ross (1974) that suggests five ν_3 bands, two ν_1 bands, three ν_4 bands, three ν_2 bands, and several water-bending and librational bands, likely because of the different sulfate-coordinated cations in the structure (K, Mg, Ca). Nonetheless, the correlation between the two spectra is simple to make because the overall shape of the spectra are very similar and the assignments of the bands given here for the emissivity spectrum agree with those presented by Ross.

Bassanite (hemihydrate) is a Ca-sulfate whose hydration state (0.5 H_2O) falls between that of anhydrite ($CaSO_4$) and gypsum ($CaSO_4 \cdot 2H_2O$). The bassanite ν_3 features (Fig. 3) occur at 1171, 1158, and 1093 cm^{-1}. The ν_1 feature is not a sharp peak, but rather is observed as the downward trend of the spectrum (at 1000 cm^{-1}) on the low-frequency side of a sharp emissivity maximum at 1011 cm^{-1}. Two distinct ν_4 bands are seen as sharp features at 664 and 600 cm^{-1} and a small additional ν_4 band occurs between them at 630 cm^{-1}. A truncated band occurs at ~240 cm^{-1} that is thought to result from a Ca-O mode (Ferraro and Walker 1965). The ν_2 bands, if present, are unclear among the spectral noise, but were identified at ~465 and ~420 cm^{-1} in the transmission spectrum of Moenke (1962) as reported by Ross (1974). All of these bands considered together do not distinguish uniquely the sulfate site symmetry between C_2 and C_1 (Ross 1974). It is unlikely, however, that the symmetry is D_2, also listed by Ross as a possibility, because an otherwise unpredicted ν_1 band is seen here that also has been identified in other works (e.g., Sarma et al. 1998, using Raman data; Prasad et al. 2005, using transmission and Raman data). An emissivity maximum at 1630 cm^{-1} represents the δH_2O mode.

The gypsum spectrum (Fig. 3) shows one obvious ν_3 mode at 1155 cm^{-1}; however, the slightly bowed non-Lorentzian shape suggests the possibility of other bands that also are predicted by the C_2 site symmetry of the sulfate tetrahedron (Hass and Sutherland 1956; Hezel and Ross 1966; Berenblut et al. 1971). In fact, several distinct ν_3 bands were seen using polarized reflectance, as demonstrated by three unique extinction coefficient maxima (Hass and Sutherland 1956). C_2 symmetry suggests there should be one ν_1 band; however, this ν_1 band is not perceptible in the emissivity spectrum, likely because the ν_1 band is very weak, as is also the case for the transmission spectrum of Moenke (1962). The simplicity of the ν_3 band(s) (i.e., the lack of splitting) sug-

gests minimal distortion. Crowley and Hook (1996) presented a gypsum spectrum acquired using directional-hemispherical reflectance that also does not show a ν_1 band, and Vassallo and Finnie (1992) showed a ν_1 band in gypsum that disappears with increasing experimental temperatures. Two ν_4 bands are seen at 676 and 604 cm^{-1} with a possible shoulder on the lower-frequency band at ~595 cm^{-1} (a third ν_4 band?), consistent with the two ν_4 bands observed in transmission by both Putnis et al. (1990) and Prasad et al. (2005), regardless of the C_2 symmetry predicting three bands. Three ν_4 bands were observed by Hass and Sutherland (1956) using a reflection technique, but two were extremely close together (at 602 and 604 cm^{-1}). A broad band is seen at ~470 cm^{-1} that was assigned by Hass and Sutherland (1956) to a water libration and their rationale is reasonable and probable; however, in Raman spectra there are two ν_2 bands that occur in much the same position (e.g., Berenblut et al. 1971; Sarma et al. 1998; Prasad et al. 2001; Knittle et al. 2001), so the sulfate ν_2 vibration may contribute to some, albeit minor, degree (Vassallo and Finnie 1992). A lattice mode occurs at longer wavelengths and is truncated at 220 cm^{-1}. In gypsum, the water molecules are quite interactive with the CaO and SO_4 groups (Sarma et al. 1998) and cause a distinct, sharp band (δH_2O) in the emissivity spectrum at 1621 cm^{-1} (e.g., Hass and Sutherland 1956).

With the addition of water in the gypsum structure, it exhibits a sheet structure, unlike bassanite and anhydrite whose chains of SO_4 tetrahedra and CaO_8 dodecahedra are in three-dimensional frameworks. Interestingly, there exists a step-wise trend in both the lattice mode and in the ν_3 band from anhydrite to bassanite to gypsum. These bands for the anhydrous Ca-sulfate occur at higher frequency than for the bassanite, and the same trend is also true between bassanite and the more-hydrated Ca-sulfate (gypsum) (Fig. 4a). In this sequence the phase transitions are associated with a structural change related to the dehydration and rehydration process (Sarma et al. 1998); however, the structural modification due to water between anhydrite and bassanite is small, so the dehydration-rehydration process is reversible. This is not true for gypsum to bassanite/anhydrite in which the dehydration-rehydration process is irreversible (Hummel et al. 2001). It is interesting to note that the same trend of the ν_3 band shifting to higher frequency (higher wavenumber) with decreasing water content also was observed in: (1) a separate emission study (M.D. Lane, unpublished) of Mg-sulfates (Fig. 4b), which included $MgSO_4 \cdot 7H_2O$, oven-dried $MgSO_4 \cdot 7H_2O$ (resulting in water loss), $MgSO_4 \cdot H_2O$ (kieserite), and anhydrous $MgSO_4$ reagent; (2) in Fe-sulfates ($FeSO_4 \cdot 4H_2O$, rozenite), under unpurged and purged conditions (Bishop et al. 2005, using emission and reflectance data); and (3) in polyhydrated, monohydrated, and anhydrous Cu-sulfates (Ferraro and Walker 1965, Table VI). Chio et al. (2004) also show this trend in Raman data for the ν_1 band, shifting to higher frequency from gypsum to bassanite to anhydrite. They suggest that, because anhydrite does not have any molecular water, the S-O bond is stronger than in gypsum. Also, the hydrogen bonding in bassanite is considerably weaker than that in gypsum due to a longer OH···O bonding distance, and the weakened hydrogen bonding in bassanite leads to a stronger S-O bond (thus the higher-frequency of the ν_1 band).

Decreasing the particle size of a mineral sample causes the fundamental vibrational band depths to shallow and in some cases to invert, and also causes volume scattering features to appear and deepen. The latter often enhances the spectral contrast associated with very weak bands, thereby allowing their position to be identified.

To study particle size effects for a sulfate mineral, a fine-grained, <10 µm powder was made of the gypsum sample and the emissivity spectrum was obtained (not shown). Differences between emissivity spectra of particulate and consolidated hand samples are due primarily to the increasing number of grain/air interfaces per unit volume with decreasing particle size and the associated increase in scattering due to reflections and refractions from both external (multiple scattering) and internal (volume scattering) sides of the grain. The fine-grained gypsum sample showed typical Type I, II, and III behaviors as defined by Hunt and Vincent (1968). Type I behavior occurred in the ν_3 region of gypsum (at ~1155 cm^{-1}). Type II behavior was seen at ~1621, ~676, and ~604 cm^{-1}. Additionally, in the transparency/volume scattering region located between the ν_3 and ν_4 bands, some sharp, Type III emissivity maxima were observed (i.e., very small, weak bands became more prominent and appeared as sharp emissivity maxima within broad emissivity troughs as particle size decreased and spectral contrast was enhanced). These sharp maxima in the fine-grained sample spectrum enabled

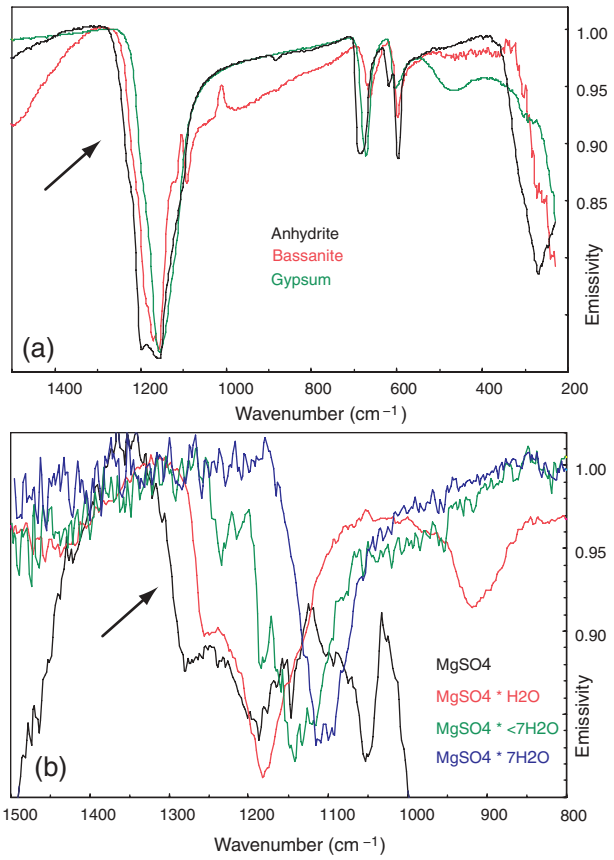

FIGURE 4. Emissivity spectra of (**a**) Ca-sulfates and (**b**) Mg-sulfates showing the shift to higher frequency (larger wavenumber) of the ν_3 (see arrow) and lattice modes (in Ca sulfates) associated with the dehydration of the mineral.

the otherwise very weak and previously unseen ν_1 feature and equally weak δOH feature to be identified in gypsum (at ~1010 and ~877 cm^{-1}, respectively).

Hydrous sulfates with additional anions

The samples of this classification (Strunz 6/D.) presented here include zincobotryogen, ferricopiapite, thaumasite, kainite, and serpierite. Both zincobotryogen and ferricopiapite are members of the copiapite group minerals. The spectra for each of these samples are shown in Figure 5.

The zincobotryogen spectrum has many bands for this complex, monoclinic salt, due to the additional presence of OH and H_2O in the structure and its low symmetry. The ν_3 bands occur at 1220, 1132, and 1031, with additional ν_3 bands at 1164 (shoulder) and 1068 cm^{-1}. These five ν_3 bands exhibited in zincobotryogen are similar to the five ν_3 bands shown for botryogen in the transmission data of Moenke (1962) as assigned by Ross (1974). The ν_1 band is small but clear at 999 cm^{-1}. It is possible that the small band at 1010 cm^{-1} is due to water in the mineral (δOH), as it occurs just to the high-frequency side of the ν_1 band, similar to that band relationship in jarosite. And a small feature at 806 cm^{-1} also could result from an OH-bending vibration. Constituent water additionally causes a bending mode (δH_2O) to be seen at 1660 cm^{-1} (e.g., Ross 1974). Three strong ν_4 bands are present at 602, 545, and 485 cm^{-1}. The ν_2 band may occur at ~393 cm^{-1} and there is a strong lattice band at ~280 cm^{-1}. Ferricopiapite, a triclinic mineral, exhibits ν_3 bands at 1220, ~1116, and 1050 cm^{-1}. The ν_1 clearly occurs at 997 cm^{-1}. The ν_4 bands occur at 600 and 552 cm^{-1}, although this latter band is assigned by Ross (1974), in the similar copiapite spectrum of Moenke (1962), to be an OH-bending mode. The ν_2 band is exhibited at ~467 cm^{-1} and a strong lattice mode is truncated at 220 cm^{-1}. The sulfate symmetry of ferricopiapite is C_1 (as it is for copiapite), which allows for one more ν_4 and one more ν_2 band than is seen in the emissivity spectrum (Fig. 5). Scattering features related to the small effective particle size of the sample also are seen as the general decrease in emissivity at >1649 cm^{-1}. One notable doublet occurs between 1649 and 1279 cm^{-1}. This doublet is due to the water present in the structure of the mineral and is pronounced due to the scattering of the emitted energy from this friable sample. The water in the structure causes the emissivity maxima at ~1649 and ~1444 cm^{-1} that result from splitting of the

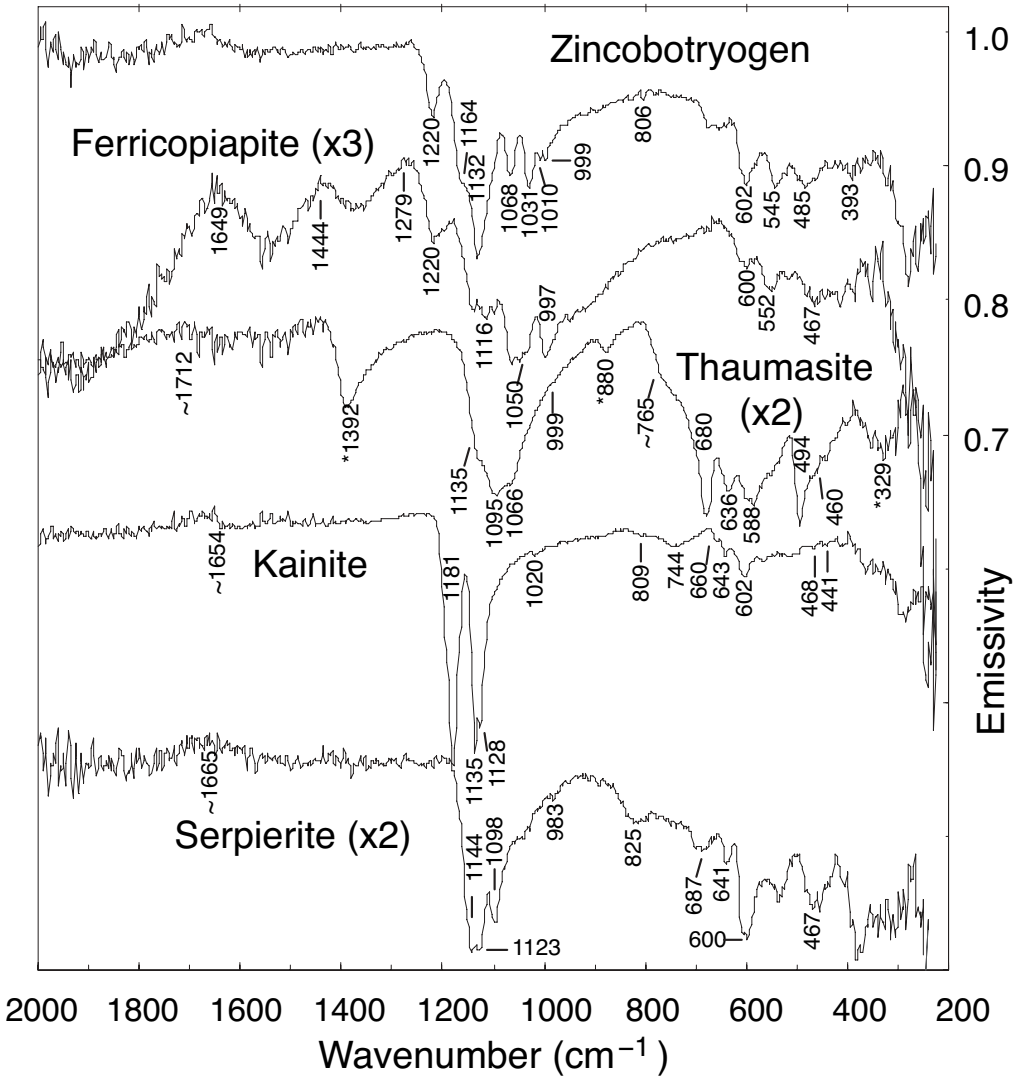

FIGURE 5. Mid-infrared thermal emissivity spectra of hydrous sulfates with additional anions, where the asterisks denote bands from carbonate in the mineral structure. The band depths of some spectra have been modified for easier comparison as noted by the parenthetical values. Spectra are offset for clarity.

H_2O deformation mode. The emissivity spectra of fine-grained szomolnokite, kieserite, coquimbite, kornelite, and a few other hydrous sulfate samples that display scattering features (none of which are shown here) also exhibit this doublet at variable wavenumber positions; however, this doublet is not seen in their coarse-particle (crystalline) counterparts [e.g., the doublet is not seen in the spectra of (para)coquimbite, kieserite, or szomolnokite samples shown in Fig. 3] nor in any fine-grained non-hydrous sulfate samples. The scattering in the emissivity spectra allows this doublet to be identified, but this doublet also is seen clearly in the transmission data for goslarite and ilesite of Moenke (1962), which also are hydrated sulfate minerals.

Thaumasite is a complex hydrated Ca-sulfate mineral (of the ettringite group) that bears anionic compounds of CO_3, SO_4, and OH in addition to the bound H_2O molecules. It is an unusual mineral in that it is the only mineral known to contain Si that coordinates with six hydroxyl groups and is stable at ambient pressures and temperatures (e.g., Edge and Taylor 1971; Lewandowska and Rospondek 2002; Jacobsen et al. 2003). The CO_3-related features occur at 1392 (CO_3 ν_3), 880 (CO_3 ν_2), and 329 (CO_3 lattice mode) cm^{-1}. The sulfate ν_3 features occur at ~1135 (shoulder), 1095, and 1066 cm^{-1}. The sulfate ν_1 appears at 999 cm^{-1}, albeit weak. And two strong sulfate ν_4 bands occur at 636, and 588 cm^{-1}. A strong sulfate lattice mode band is truncated at the long-wavelength end of the spectrum. The spectral features that result from the Si-O vibrations in the unusual $Si(OH)_6^{2-}$ groups occur at: ~765 cm^{-1} (very broad shoulder) due to Si-O stretching, 680 cm^{-1} (also due to νSi-O), and two δSi-O bending modes at 494 and ~460 cm^{-1} (shoulder) (Lewandowska and Rospondek 2002, using transmission data). The δH_2O mode occurs at ~1712 cm^{-1} as an emissivity maximum (e.g., Lewandowska and Rospondek 2002).

The chemical formula of kainite may be written as $MgSO_4 \cdot KCl \cdot 3H_2O$, which identifies the constituent chloride and sulfate components. Kainite is one of the few sulfates that contains chloride. Chlorides typically do not exhibit spectral features in the infrared and, accordingly, the spectral features of kainite are all associated with the sulfate and water vibrations. Three strong and sharp ν_3 features are exhibited at 1181, 1135, and 1128 cm^{-1}. The ν_1 feature occurs at 1020 cm^{-1}. Three discrete ν_4 features occur at 660, 643, and 602 cm^{-1}. A ν_2 mode is exhibited at 468 cm^{-1} and a second ν_2 may occur at ~441 cm^{-1}. A sulfate lattice mode is truncated at the long-wavelength edge of the spectrum. Water vibrations are seen at ~1654 cm^{-1} (δH_2O) (e.g., Omori and Kerr 1963) and at 809 and 744 cm^{-1} (both δOH modes). The amount of sulfate anion bands seen, and the low number of degeneracies, suggests a fairly low site symmetry perhaps as high as C_{2v} (if only one ν_2 band) and as low as C_1.

The sample of serpierite used for this study was a small (~5 × 5 mm) bluish crystal growth on a larger substrate that was masked during data acquisition. Overall there is a slope in this spectrum that is due to sample cooling during the scanning (Fig. 5). Despite the slope in the spectrum, the spectral features of the monoclinic serpierite sample are clear. There are numerous spectral features in this complex Cu sulfate due to the presence of both OH and H_2O in the structure and the mineral's lack of symmetry. The emissivity features in Figure 5 occur as follows: three ν_3 features at 1144, 1123, and 1098 cm^{-1}; a clear ν_1 mode at 983 cm^{-1}; two clear ν_4 features at 641 and 600 cm^{-1}; and a broad band at ~467 cm^{-1} with superposed structure that represents the region of ν_2 with an unclear number of bands. The Moenke (1966) transmission data discussed in Ross (1974) show a similar number of bands: three ν_3 bands at 1125, 1108, and 1065 cm^{-1}; a ν_1 at 990 cm^{-1}; two ν_4 at 648 and 610 cm^{-1}; however, unlike the emissivity spectrum, the Moenke (1966) data show two discrete ν_2 bands at 475 and 445 cm^{-1}. The Raman spectrum from Frost et al. (2004) also is similar in the number of bands: three ν_3 bands at 1131, 1122, and 1077 cm^{-1}; a ν_1 at 988 cm^{-1}; two ν_4 at 645 and 605 cm^{-1}; however, unlike the emissivity spectrum, the Frost et al. (2004) data show three discrete ν_2 bands at 475, 445, and 421 cm^{-1}. A lattice mode in the emissivity spectrum (Fig. 5) occurs at $\gtrsim$400 cm^{-1}. As a result of the water in the serpierite, a water-bending mode occurs as an emissivity maximum at ~1665 cm^{-1} and two δOH modes are seen at 825 and 687 cm^{-1}. These three water modes were also shown in Moenke (1966) as assigned by Ross (1974).

Sulfate-bearing minerals (not officially sulfates)

Although not officially "sulfates," some minerals contain a sulfate anion group in their structure and display sulfate anion vibrational modes in their mid-infrared spectra (Fig. 6). The samples of this classification presented here include creedite (a fluoride group halide; Strunz 3/C.) and afghanite (a cancrinite

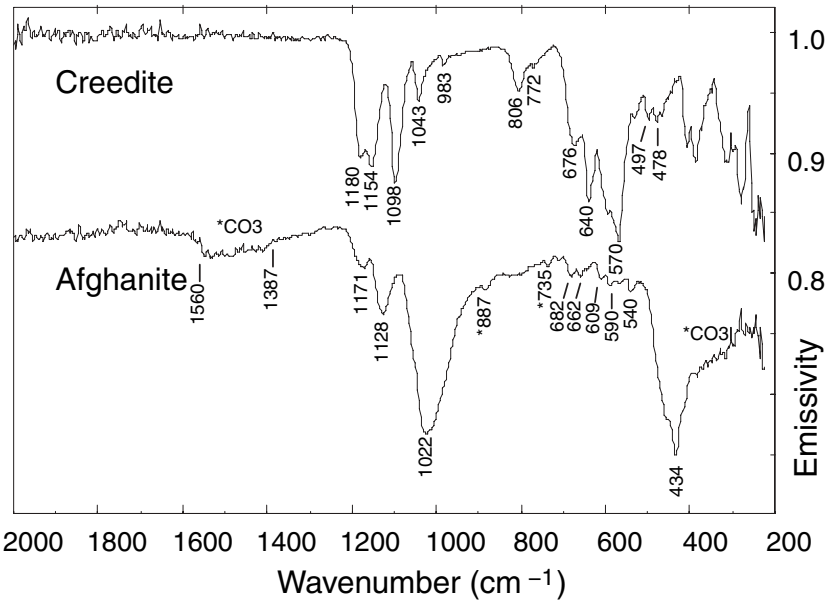

FIGURE 6. Mid-infrared thermal emissivity spectra of sulfate-bearing minerals that are not officially sulfates, where the asterisks denote bands from carbonate in the mineral structure. Spectra are offset for clarity.

group silicate; Strunz 8/J.).

The creedite spectrum (Fig. 6) exhibits and is dominated by a large number of absorption features related to the vibrations of the sulfate anion. Features at 1180, 1154, 1098, and 1043 cm^{-1} result from sulfate ν_3 vibrations. A distinct ν_1 feature occurs at 983 cm^{-1}, three ν_4 features are seen at 676, 640, and 570 cm^{-1}, and two ν_2 features are seen at 497 and 478 cm^{-1}. The water in the structure causes bands to arise at 806 and 772 cm^{-1} due to δOH.

The mineral structure of afghanite is described in detail in Ballirano et al. (1996). The afghanite emissivity spectrum (Fig. 6) contains features related to the carbonate and sulfate anionic groups in the structure. The carbonate features include the broad CO_3 ν_3 absorption from ~1560 to 1387 cm^{-1}, the CO_3 ν_2 at 887 cm^{-1}, and the CO_3 ν_4 at 735 cm^{-1}. The breadth of the long-wavelength lattice band at ~400 to 250 cm^{-1} likely is due to the superposed carbonate lattice mode on a sharper metal-O mode at 434 cm^{-1}. The sulfate anion features include three ν_3 modes at 1171, 1128, and 1022 cm^{-1}. The ν_1 mode is not distinct. The sulfate ν_4 bands occur at 609 and 590 cm^{-1}. It is also possible that the band at 540 cm^{-1} represents a ν_4 vibration. The features at 682 and 662 cm^{-1} may represent Si-Al-O bending modes (Ballirano et al. 1996). As discussed for the kainite spectrum above, the Cl in the mineral does not exhibit specific features in the spectrum.

Final remarks

Sulfate anions in minerals may exhibit bands in the IR at ~1050–1250 (ν_3), ~1000 (ν_1), ~500–700 (ν_4), and ~400–500 (ν_2) cm^{-1} due to asymmetric and symmetric stretching and bending of the SO_4 anion. The number and position of the fundamental bands are dependent upon the sulfate symmetry and the degree of deformation of the anion. Additional spectral emissivity features may arise due to OH and H_2O in the molecular structure of some sulfates. Several sulfates also contain anionic carbonate in the structure that causes additional spectral emissivity features; however, constituent Cl does not cause spectral bands to arise.

The amount of hydration in minerals with similar chemistry will affect the high-frequency position of the ν_3 fundamental bands. This position change is seen in the Ca-, Mg-, Fe-, and Cu-sulfate series in which the ν_3 band occurs at a lower-frequency (lower wavenumber) position with higher states of hydration.

A water librational band that occurs at 846 cm^{-1} in szomolnokite and 919 cm^{-1} in kieserite is unique in appearance and restricted to these two monohydrated sulfates studied here. It is predicted that this band will be present in the emissivity spectra of other monoclinic kieserite-group sulfates (e.g., szmikite, gunningite) and may be used as an indicator for monohydrated sulfates.

Finally, particle size also affects the sulfate spectra, as discussed for gypsum, and fine-grained sulfates can exhibit Type I, II, and III band behaviors. Coarse, crystalline samples exhibit spectra dominated by the absorption bands associated with the fundamental vibrational modes of the constituent anion(s), whereas fine-grained samples have spectra that can be dominated by multiple- and volume-scattering features and show diminished or inverted fundamental modes. As a result of the inversion of fundamental bands and neighboring increased spectral contrast, the position of previously indistinct vibrational modes may be discerned in fine-grained samples.

The unique spectral character of sulfates (and sulfate-bearing minerals) allows their emissivity spectra to be used for identification of these minerals, spectral determination of unknown composition, and in some cases, identification of the physical state of the mineral (coarse vs. particulate). Knowing these characteristics can provide insight into the geologic setting in which they are found, whether by fieldwork or through airborne or orbital remote sensing techniques.

Acknowledgments

Thanks are extended to James Talbot at K/T GeoServices, Inc. for his assistance with the majority of the XRD analyses. I also thank Darby Dyar, Vanessa O'Connor, and Gerard Marchand at Mount Holyoke College, and David Bish (Indiana University) for their assistance with a few additional XRD analyses, and Janice Bishop (SETI/NASA-Ames) for the rozenite sample. Additional thanks are extended to Vicky Hamilton, Ray Arvidson, and Brigitte Wopenka for their reviews of this manuscript that improved the readability of the final paper. This work (PSI contribution no. 383) was funded through the NASA Mars Odyssey Participating Scientist Program and the NASA Mars Fundamental Research Program.

References cited

Adler, H.H. and Kerr, P.F. (1965) Variations in infrared spectra, molecular symmetry and site symmetry of sulfate minerals. American Mineralogist, 50, 132–147.

Araki, T. (1961) Crystal structure of antlerite. Mineralogy Journal (Tokyo), 3, 233–235.

Aronson, J.R. and Emslie, A.G. (1973) Spectral reflectance and emittance of particulate materials, 2, Application and results. Applied Optics, 12, 2573–2584.

Aronson, J.R., Emslie, A.G., and McLinden, H.G. (1966) Infrared spectra from particulate surfaces. Science , 152, 345–346.

Aronson, J.R., Emslie, A.G., Allen, R.V., and McLinden, H.G. (1967) Studies of the middle- and far-infrared spectra of mineral surfaces for application in remote compositional mapping of the Moon and planets. Journal of Geophysical Research, 72, 687–703.

Aronson, J.R., Miseo, E.V., Smith, E.M., Emslie, A.G., and Strong, P.F. (1983) Optical constants of monoclinic anisotropic crystals—Gypsum. Applied Optics, 22, 4093–4098.

Ballirano, P., Maras, A., and Buseck, P.R. (1996) Crystal chemistry and IR spectroscopy of Cl- and SO_4-bearing cancrinite-like minerals. American Mineralogist, 81, 1003–1012.

Berenblut, B.J., Dawson, P., and Wilkinson, G.R. (1971) The Raman spectrum of gypsum. Spectrochimica Acta, 27A, 1849–1863.

Bishop, J.L. and Murad, E. (2005) The visible and infrared spectral properties of jarosite and alunite. American Mineralogist, 90, 1100–1107.

Bishop, J.L., Dyar, M.D., Lane, M.D., and Bandfield, J. (2005) Spectral identification of hydrated sulfates on Mars and comparison with acidic environments on Earth. International Journal of Astrobiology, 3(4), 275–285.

Breitinger, D.K., Krieglstein, R., Bogner, A., Schwab, R.G., Pimpl, T.H., Mohr, J., and Schukow, H. (1997) Vibrational spectra of synthetic minerals of the alunite and crandallite type. Journal of Molecular Structure, 408/409, 287–290.

Burgio, L. and Clark, R.J.H. (2001) Library of FT-Raman spectra of pigments, minerals, pigment media and varnishes, and supplement to existing library of Raman spectra of pigments with visible excitation. Spectrochimica Acta, A57, 1491–1521.

Campbell, J.A., Ryan, D.P., and Simpson, L.M. (1970) Interionic forces in crystals—II. Infrared spectra of SO_4 groups and "octahedrally" coordinated water in some alums, Tutton salts, and the double salts obtained by dehydrating them. Spectrochimica Acta, 26A, 2351–2361.

Chio, C.H., Sharma, S.K., and Muenow, D.W. (2004) Micro-Raman studies of gypsum in the temperature range between 9 and 373 K. American Mineralogist, 89, 390–395.

Christensen, P.R. and Harrison, S.T. (1993) Thermal infrared emission spectroscopy of natural surfaces: Application to desert varnish coatings on rocks. Journal of Geophysical Research, 98, 19819–19834.

Christensen, P.R. and 25 others (2001) The Mars Global Surveyor Thermal Emission Spectrometer experiment: Investigation description and surface science results. Journal of Geophysical Research, 106, 23823–23871.

Christensen, P.R. and 19 others (2003) Miniature Thermal Emission Spectrometer for the Mars Exploration Rovers. Journal of Geophysical Research, 108 (E12), 8064, DOI: 10.1029/2003JE002117.

Christensen, P.R., Jakosky, B.M., Kieffer, H.H., Malin, M.C., McSween, H.Y., Jr., Nealson, K., Mehall, G.L., Silverman, S.H., Ferry, S., Caplinger, M., and Ravine, M. (2004) The Thermal Emission Imaging System (THEMIS) for the Mars 2001 Odyssey Mission. Space Science Reviews, 100, 85–130.

Clark, R.N. (1999) Chapter 1: Spectroscopy of Rocks and Minerals, and Principles of Spectroscopy. In A.N. Rencz, Ed., Manual of Remote Sensing, Remote Sensing

for the Earth Sciences, 3, p. 3–58. John Wiley and Sons, New York.
Conel, J.E. (1969) Infrared emissivities of silicates: Experimental results and a cloudy atmosphere model of spectral emission from condensed particulate mediums. Journal of Geophysical Research, 74, 1614–1634.
Cooper, B.L., Salisbury, J.W., Killen, R.M., and Potter, A.E. (2002) Midinfrared spectral features of rocks and their powders. Journal of Geophysical Research, 107 (E4), 5017, DOI: 10.1029/2001JE001462.
Crowley, J.K. and Hook, S.J. (1996) Mapping playa evaporite minerals and associated sediments in Death Valley, California, with multispectral thermal infrared images. Journal of Geophysical Research, 101, 643–660.
Edge, R.A., and Taylor, H.F.W. (1971) Crystal structure of thaumasite, $[Ca_3Si(OH)_6 \cdot 12H_2O](SO_4)(CO_3)$. Acta Crystallographica, B27, 594–601.
Ferraro, J.R. and Walker, A. (1965) Comparison of the infrared spectra (4000–70 cm^{-1}) of several hydrated and anhydrous salts of transition metals. Journal of Chemical Physics, 42(4), 1278–1285.
Frost, R.L. and Kloprogge, J.T. (2001) Raman microscopy of kalinite and tschermigite and lonecreekite at 298 and 77 K. Neues Jahrbuch für Mineralogie, Monatshefte, 27–40.
Frost, R.L., Kloprogge, J.T., Williams, P.A., and Leverett, P. (2000) Raman microscopy of some natural pseudo-alums: halotrichite, apjohnite, and wupatkiite, at 298 and 77 K. Journal of Raman Spectroscopy, 31, 1083–1087.
Frost, R.L., Williams, P.A., Martens, W., Leverett, P., and Kloprogge, J.T. (2004) Raman spectroscopy of basic copper (II) and some complex copper (II) sulfate minerals: Implications for hydrogen bonding. American Mineralogist, 89, 1130–1137.
Frost, R.L., Weier, M.L., Kloprogge, J.T., Rull, F., and Martinez-Frias, J. (2005) Raman spectroscopy of halotrichite from Jaroso, Spain. Spectrochimica Acta, 62 A, 176–180, DOI: 10.1016/j.saaa.2004.12.023.
Gadsden, J.A. (1975) Infrared Spectra of Minerals and Related Inorganic Compounds, p. 75. Butterworths, England.
Griffen, D.T. and Ribbe, P.H. (1979) Distortions in the tetrahedral oxyanions of crystalline substances. Neues Jahrbuch für Mineralogie, Abhandlungen, 137, 54–73.
Grodzicki, A. and Piszczek, P. (1998) A new interpretation of abnormal shift of water molecules' bending vibration frequencies in kieserite family monohydrates. Journal of Molecular Structure, 443, 141–147.
Hass, M. and Sutherland, G.B.B.M. (1956) The IR spectra and crystal structure of gypsum. Proceedings of the Royal Society of London, 236A, 427–445.
Hawthorne, F.C., Groat, L.A., and Eby, R.K. (1989) Antlerite, $Cu_3SO_4(OH)_4$, a heteropolyhedral wallpaper structure. Canadian Mineralogist, 27, 205–209.
Hawthorne, F.C., Krivovichev, S.V., and Burns, P.C. (2000) The crystal chemistry of sulfate minerals. In C.N. Alpers, J.L. Jambor, and D.K. Nordstrom, Eds., Sulfate Minerals: Crystallography, Geochemistry, and Environmental Significance, 40, p. 1–112. Reviews in Mineralogy and Geochemistry, Mineralogical Society of America, Chantilly, Virginia.
Herzberg, G. (1945) Infrared and Raman Spectra of Polyatomic Molecules. Van Nostrand, New York.
Hezel, A. and Ross, S.D. (1966) Forbidden transitions in the infra-red spectra of tetrahedral anions—III. Spectra-structure correlations in perchlorates, sulphates and phosphates of the formula MXO_4. Spectrochimica Acta, 22, 1949–1961.
Huang, C.K. and Kerr, P.F. (1960) Infrared study of the carbonate minerals. American Mineralogist, 45, 311–324.
Hug, S.J. (1997) In situ Fourier transform infrared measurements of sulfate adsorbed on hematite in aqueous solutions. Journal of Colloid and Interface Science, 188, 415–422.
Hummel, H.U., Abdussaljamow, B., Fischer, H.B., and Stark, J. (2001) Examination of the hygro-mechanical stability of crystalline calcium sulfate hemihydrate, Part 1. ZKG International, 54, 272–278.
Hunt, G.R. and Logan, L.M. (1972) Variation of single particle mid-infrared emission spectrum with particle size. Applied Optics, 11, 142–147.
Hunt, G.R. and Vincent, R.K. (1968) The behavior of spectral features in the infrared emission from particulate surfaces of various grain sizes. Journal of Geophysical Research, 73, 6039–6046.
Jacobsen, S.D., Smyth, J.R., and Swope, R.J. (2003) Thermal expansion of hydrated six-coordinated silicon in thaumasite, $Ca_3Si(OH)_6(CO_3)(SO_4) \cdot 12H_2O$. Physics and Chemistry of Minerals, 30, 321–329.
Jambor, J.L., Nordstrom, D.K., and Alpers, C.N. (2000) Metal-sulfate salts from sulfide mineral oxidation. In C.N. Alpers, J.L. Jambor, and D.K. Nordstrom, Eds. Sulfate Minerals: Crystallography, Geochemistry, and Environmental Significance, 40, p. 303–350. Reviews in Mineralogy and Geochemistry, Mineralogical Society of America, Chantilly, Virginia.
Knittle, E., Phillips, W., and Williams, Q. (2001) An infrared and Raman spectroscopic study of gypsum at high pressures. Physics and Chemistry of Minerals, 28, 630–640.
Lane, M.D. (1999) Midinfrared optical constants of calcite and their relationship to particle size effects in thermal emission spectra of granular calcite. Journal of Geophysical Research, 104, 14099–14108.
Lane, M.D. and Christensen, P.R. (1997) Thermal infrared emission spectroscopy of anhydrous carbonates. Journal of Geophysical Research, 102, 25581–25592.
——— (1998) Thermal infrared emission spectroscopy of salt minerals predicted for Mars. Icarus, 135, 528–536.
Lane, M.D., Dyar, M.D., and Bishop, J.L. (2004) Evidence for hydrous iron sulfate in the Martian soil. Geophysical Research Letters, 31, L19702, DOI: 10.1029/2004GL021231.
Lazaroff, N., Sigal, W., and Wasserman, A. (1982) Iron oxidation and precipitation of ferric hydroxysulfates by resting Thiobacillus ferrooxidans cells. Applied and Environmental Microbiology, 43(4), 924–938.
Lewandowska, A. and Rospondek, M. (2002) Thaumasite—A rare mineral containing $Si(OH)_6^{2-}$ groups from Dubie (the Dębnik anticline, S. Poland). Mineralogia Polonica, 33(1), 25–34.
Libowitzky, E. (1999) Correlation of O-H stretching frequencies and O-H···O-H bond lengths in minerals. Monatshefte für Chemie, 130, 1047–1059.
Lyon, R.J.P. (1964) Evaluation of infrared spectrophotometry for compositional analysis of lunar and planetary soils, II, Rough and powdered surfaces. NASA Conference Report CR-100.
Makreski, P., Jovanovski, G., and Dimitrovska, S. (2005) Minerals from Macedonia: XIV. Identification of some sulfate minerals by vibrational (infrared and Raman) spectroscopy. Vibrational Spectroscopy, 39(2), 229–239.
Martens, W., Frost, R.L., Kloprogge, J.T., and Williams, P.A. (2003) Raman spectroscopic study of the basic copper sulphates—implications for copper corrosion and "bronze disease." Journal of Raman Spectroscopy, 34, 145–151.
Miller, F.A., Carlson, G.L., Bentley, F.F., and Jones, W.H. (1960) Infrared spectra of inorganic ions in the cesium bromide region (700–300 cm^{-1}). Spectrochimica Acta, 16, 135–235.
Mitra, S.S. (1963) Combination of the lattice modes with the internal modes in a crystal. Journal of Chemical Physics, 39(11), 3031–3033.
Moenke, H. (1959) Ultrarot-spektralphotometrische Bestimmung der gesteinsbildenen Saltzmineralien. Jenaer Jahrbuch, 2, 361–395.
——— (1962) Mineralspektren I: Die Ultrarotabsorption der häufigsten und wirtschaftlich wichtigsten Halogenid-, Oxyd-, Hydroxyd-, Carbonat-, Nitrat-, Borat-, Sulfat-, Chromat-, Wolframat-, Molybdat-, Phosphat-, Arsenat-, Vanadat- und Silikatmineralien im Spektralbereich 400–4000 cm^{-1}. Akademie Verlag, Berlin.
——— (1966) Mineralspektren II: Die Ultrarotabsorption häufiger und paragenetisch oder wirtschaftlich wichtiger Carbonate-, Borat-, Sulfat-, Chromat-, Phosphat-, Arsenat-, und Vanadat- und Silikatmineralien im Spektralbereich 400–4000 cm^{-1} (25–2.5 μm). Akademie Verlag, Berlin.
Moersch, J.E. (1992) Modeling Particle Size Effects on the Emissivity Spectra of Minerals in the Thermal Infrared. M.S. thesis, Arizona State University, Tempe.
Moersch, J.E. and Christensen, P.R. (1995) Thermal emission from particulate surfaces: A comparison of scattering models with measured spectra. Journal of Geophysical Research, 100, 7465–7477.
Mustard, J.F. and Hays, J.E. (1997) Effects of hyperfine particles on reflectance spectra from 0.3 to 25 μm. Icarus, 125, 145–163.
Nakamoto, K. (1986) Infrared and Raman Spectra of Inorganic and Coordination Compounds. Wiley and Sons, New York.
Omori, K. (1970) Infrared study of sulfohalite. American Mineralogist, 55, 18997–1910.
Omori, K. and Kerr, P.F. (1963) Infrared studies of saline sulfate minerals. Geological Society of America Bulletin, 74, 709–734.
Powers, D.A., Rossman, G.R., Schugar, H.J., and Gray, H.B. (1975) Magnetic behavior and infrared spectra of jarosite, basic iron sulfate, and their chromate analogs. Journal of Solid State Chemistry, 13, 1–13.
Prasad, P.S.R., Pradhan, A., and Gowd, T.N. (2001) In situ micro-Raman investigation of dehydration mechanism in natural gypsum. Current Science, 80(9), 1203–1207.
Prasad, P.S.R., Krishna Chaitanya, V., Shiva Prasad, K., and Narayana Rao, D. (2005) An intermediate γ-$CaSO_4$ phase in dehydration process of gypsum: In-situ FTIR study. American Mineralogist, 90, 672–678.
Putnis, A., Winkler, B., and Fernandez-Diaz, L. (1990) In situ IR spectroscopic and thermogravimetric study of the dehydration of gypsum. Mineralogical Magazine, 54, 123–128.
Ross, S.D. (1974) Sulfates and other oxy-anions of Group VI. In V.C. Farmer, Ed., The Infrared Spectra of Minerals, p. 423–444. Mineralogical Society, London.
Ruff, S.W., Christensen, P.R., Barbera, P.W., and Anderson, D.L. (1997) Quantitative thermal emission spectroscopy of minerals: A laboratory technique for measurement and calibration. Journal of Geophysical Research, 102, 14899–14913.
Salisbury, J.W. and Eastes, J.W. (1985) The effect of particle size and porosity on spectral contrast in the mid-infrared. Icarus, 64, 586–588.
Salisbury, J.W. and Wald, A. (1992) The role of volume scattering in reducing spectral contrast of reststrahlen bands in spectra of powdered minerals. Icarus, 96, 121–128.
Sarma, L.P., Prasad, P.S.R., and Ravikumar, N. (1998) Raman spectroscopic study of phase transitions in natural gypsum. Journal of Raman Spectroscopy, 29, 851–856.
Sasaki, K., Tanaike, O., and Konno, H. (1998) Distinction of jarosite-group com-

pounds by Raman spectroscopy. Canadian Mineralogist, 36, 1225–1235.
Schmidt, M. and Lutz, H.D. (1993) Hydrogen bonding in basic copper salts: A spectroscopic study of malachite, $Cu_2(OH)_2CO_3$, and brochantite, $Cu_4(OH)_6SO_4$. Physics and Chemistry of Minerals, 20, 27–32.
Sejkora, J. and Ďuda, R. (1998) Natroalunite and natrojarosite from Saca (Košice region, Slovakia). Mineralia Slovaca, 30, 315–320.
Serna, C.J., Cortina, C.P., and Ramos, J.V.G. (1986) Infrared and Ramen study of alunite-jarosite compounds. Spectrochimica Acta, 42A, 729–834.
Shokarev, M.M., Margulis, E.V., Vershinina, F.I., Beisekeeva, L.I., and Savchenko, L.A. (1972) Infrared spectra of iron (III) hydroxide suphates and hydroxides. Journal of Inorganic Chemistry, 17(9), 1293–1296.
Squyres, S.W. and Knoll, A.H. (2005) Sedimentary rocks at Meridiani Planum: Origin, diagenesis, and implications for life on Mars. Earth and Planetary Science Letters, 240, 1–10.
Squyres, S.W., Grotzinger, J.P., Arvidson, R.E., Bell, J.F., III, Calvin, W., Christensen, P. R., Clark, B.C., Crisp, J.A., Farrand, W.H., Herkenhoff, K.E., Johnson, J.R., Klingelhofer, G., Knoll, A.H., McLennan, S.M., McSween, H.Y., Jr., Morris, R.V., Rice, J.W., Jr., and Soderblom, L.A. (2004) In situ evidence for an ancient aqueous environment at Meridiani Planum, Mars. Science, 306, 1709–1714.
Steger, E. and Schmidt, W. (1964) Infrarotspektren von Sulfaten und Phosphaten. Berichte der Bunsengesellschaft für Physikalische Chemie, 68, 102–109.
Stoilova, D. and Lutz, H. D. (2002) Infrared study of the vibrational behavior of the S-O stretching modes in kieserite-type selenates $MeSeO_4 \cdot H_2O$ with matrix-isolated SO_4^{2-} and Me'^{2+} guest ions (Me = Mn, Co, Ni, Zn). Journal of Molecular Structure, 606, 267–272.
Strunz, H. and Nickel, E. (2001) Strunz Mineralogical Tables: Chemical Structural Mineral Classification System (9th edition), p. 870. E. Schweizerbart'sche Verlagsbuchhandlung, Stuttgart.
Urey, H.C. and Bradley, C.A. (1931) The vibrations of pentatonic tetrahedral molecules. Physical Review, 38, 1969–1978.
Vaniman, D.T., Bish, D.L., Chipera, S.J., Fialips, C.I., Carey, J.W., and Feldman, W.C. (2004) Magnesium sulphate salts and the history of water on Mars. Nature, 431, 663–665.
Vassallo, A.M. and Finnie, K.S. (1992) Infrared emission spectroscopy of some sulfate minerals. Applied Spectroscopy, 46, 1477–1482.
Vincent, R.K. and Hunt, G.R. (1968) Infrared reflectance from mat surfaces. Applied Optics, 7, 53–59.
Wald, A.E. (1994) Modeling thermal infrared (2-14 microns) reflectance spectra of frost and snow. Journal of Geophysical Research, 94, 24241–24250.
Wald, A.E. and Salisbury, J.W. (1995) Thermal infrared directional emissivity of powdered quartz. Journal of Geophysical Research, 100, 24665–24675.
Washington, H.S. and Merwin, H.E. (1921) Aphthitalite from Kilauea. American Mineralogist, 6, 121–125.
Wenrich, M.L. and Christensen, P.R. (1996) Optical constants of minerals derived from emission spectroscopy: Application to quartz. Journal of Geophysical Research, 101, 15921–15931.
White, W.B. (1974) The carbonate minerals. In V.C. Farmer, Ed., The Infrared Spectra of Minerals, p. 227–284, Mineralogical Society, London.
Wylde, J.J., Allen, G.C., and Collins, I.R. (2001) FT-IR and Raman spectroscopic characterization of the major oilfield sulfate scale forming minerals. Applied Spectroscopy, 55(9), 1155–1160.

MANUSCRIPT RECEIVED NOVEMBER 25, 2005
MANUSCRIPT ACCEPTED JUNE 4, 2006
MANUSCRIPT HANDLED BY BRIGITTE WOPENKA